International Journal of Computer Information Systems and Industrial Management Applications
ISSN 2150-7988 Volume 18(18s) 2026 pp. 559-588
https://doi.org/10.70917/ijcisim-2026-4888
Article

The Impact of Back-Contact Materials and Absorber Layer Optimization on the Efficiency of Silicon and Tin-Based Perovskite Solar Cells-A SCAPS-1D Comparative Study

Shrutika Sharma[1*], Amit Saxena[1]

[1]Department of science, Oriental University, Indore (M.P.), India
*Correspondence Author: shrutikasharma452012@gmail.com

Abstract: Photovoltaic technology has evolved at a very higher rate and this has generated the enthusiasm to make solar cells efficient and environmental friendly. The paper provides a numerical evaluation of three solar cell designs based on the SCAPS-1D simulator tool with the purpose of discovering the impact of the choice of materials and device characteristics on the performance. The initial one is interested in a silicon-based solar cell, in which various back contact materials, including gold, copper, silver, iron, and graphene, are considered. It has been noted that metals of greater work functions are better at collecting charge and minimizing recombination losses, resulting in an ultimate efficiency of approximately 19.33. The second model focuses on a lead-free perovskite solar cell, the design of transport layers, and optimization of the absorber. In spite of the excellent optical absorption characteristics of this configuration with quantum efficiency up to almost 95, total performance is constrained by recombination losses and a reduced fill factor, leading to a low efficiency of approximately 18.63. The third model is an optimized lead-free perovskite structure that is built on $CH_3NH_3SnBr_3$, in which various parameters are optimized. This causes better transportation of the charge and the increased efficiency of about 23.2. Temperature measurement also shows that higher temperature lowers the performance of the device as a result of the increased recombination. In general, the paper demonstrates the value of optimization of materials, organization, and the conditions of work.

Keywords: Solar Cell Simulation, SCAPS-1D, Lead-Free Perovskite, $CH_3NH_3SnBr_3$, Back Contact Engineering, Quantum Efficiency, Recombination Losses, Thin Film Solar Cells, Transport Layer Optimization, Photovoltaic Efficiency

1. INTRODUCTION

The past years have seen the rising demand of clean and sustainable energy that has also contributed to a rise in research in the field of photovoltaic (PV) technologies. Solar energy is one of the most viable alternatives to fossil energy of the possibilities available since it is abundant and environmentally friendly. In the last ten years, the efficiency of solar cells, as well as a decrease in the cost of manufacturing, have facilitated the proliferation of photovoltaic systems in the global population [1,2]. Silicon-based solar cells still prevail in the business world due to their reliability and well-known fabrication methods. Nevertheless, their performance is reaching theoretical maximums, which has prompted scientists to seek new materials and novel design of devices [1]. Here, perovskite and thin-film solar cells have also received a lot of interest because they have a good absorption capacity, yet can be tuned to a wide range of bandgaps and their cost of production is comparatively low [3–5]. Specifically, organometal halide perovskites have demonstrated a rapid development, and the power conversion efficiencies have surpassed 25 percent in a few short years [3,4]. They exhibit good performance which is mainly because of good optoelectronic features including long carrier diffusion lengths, high mobility and low recombination losses [12,14].

Although these have these benefits, the existence of lead which is a toxic element in the traditional form of perovskite contributes to serious environmental and health implications, limiting their practical use [20].

Consequently, recent investigations have turned into lead-free materials, primarily tin-based perovskites like $CH_3NH_3SnBr_3$ and $CsSnI_3$, which are viewed as more acceptable in terms of the environment without a significant change in optical characteristics [20,33]. Nevertheless, such materials are usually characterized by increased defect densities and heightened recombination which lower the performance of the devices [14,33]. Besides the type of absorber material, the selection of transport layers and contact material also has a significant effect on the solar cell performance. TiO_2, ZnO, and SnO_2 are electron transport layers that help in effective electron extraction, whereas NiOx and Spiro-OMeTAD are hole transport layers that enhance efficient hole collection and stability of the device [7,911,17]. Front contacts FTO, being a transparent material, is often utilized as a transparent conductive material due to their conductivity and light transmission capabilities [23,24].

Energy band alignment at material interfaces is also another important factor. With correct alignment, the charge carriers can be separated easily and recombination losses reduced, resulting in an improved open-circuit voltage and fill factor [8]. Conversely, lack of proper alignment may lead to the accumulation of carriers and waste of their efficiency. The process of recombination, such as the Shockley ReadHall, radiative, and Auger processes also has the important role in the overall performance of the devices and should be properly regulated [15,16]. Effects of temperature cannot be disregarded because rise in temperature usually causes rise in carrier recombination and drop in open-circuit voltage, which eventually results in decrease in efficiency [2]. Hence, thermal stability is a significant factor in the design of a solar cell. Simulation tools have become very popular to analyse and optimize such complex systems. One of the most popular tools to model solar cell in thin film is SCAPS-1D because it enables one to analyze the carrier transport, recombination, and generation of the structure on a multilayer basis [17]. It offers the flexibility to investigate the effect of different parameters including layer thickness, material properties, temperature and contact design. It has been proven that SCAPS-based simulations can be useful in determining the performance-limiting factors and enhance the effectiveness of devices with the help of systematic optimization [18,19,32].

Different solar cell structures are simulated in this work, where a multi-model simulation method is applied to silicon-based devices and lead-free perovskite structures. The attention is paid to the assessment of the impact of back contact materials, the absorber thickness, the optimization of the transport layer, and temperature changes. The objective is to identify appropriate design conditions that can enhance performance whilst being environmental friendly. In general, the results of this paper can be considered as a valuable guide towards creation of effective and stable lead-free solar cells, with a significant emphasis on material and structural optimization in the forthcoming photovoltaic systems.

2. METHODOLOGY

2.1 Simulation Framework and Tool

To simulate the proposed structures of solar cells, the Solar Cell Capacitance Simulator (SCAPS-1D), a popular numerical simulation, has been used in this study which is a software designed at the University of Ghent to analyze the characteristics of thin-film photovoltaic devices. SCAPS-1D is used to solve the basic equations of semiconductor, Poisson equation, continuity equations of electrons and holes at steady state. The carrier transport mechanisms in multilayer structures are characterized by these equations in which electric fields and concentration gradients drive the process.

The physical processes that are governing the simulation are carrier generation, recombination and transport. Several recombination mechanisms that will be considered in this study are Shockley-Read-Hall, Radiative and Auger recombination. The mechanisms are important in shaping the overall device performance in that they affect carrier lifetime and recombination losses. SCAPS-1D has been chosen because it is robust in dealing with heterojunction solar cells, it can deal with defect states, and can simulate a wide range of combinations of materials and configurations of layers. The software gives a comprehensive output data which includes currentvoltage (JV) characteristics, quantum efficiencies (QE) and recombination profiles, which are vital in performance measurement and improvement.

2.2 Device Architecture Design (All Models Overview)

The simulated solar cell design used in this paper takes the shape of a multilayer design comprising of a front contact, electron transport layer (ETL), absorber layer, hole transport layer (HTL), and a back contact. Figure 1 displays the overall structure to be used in simulation.

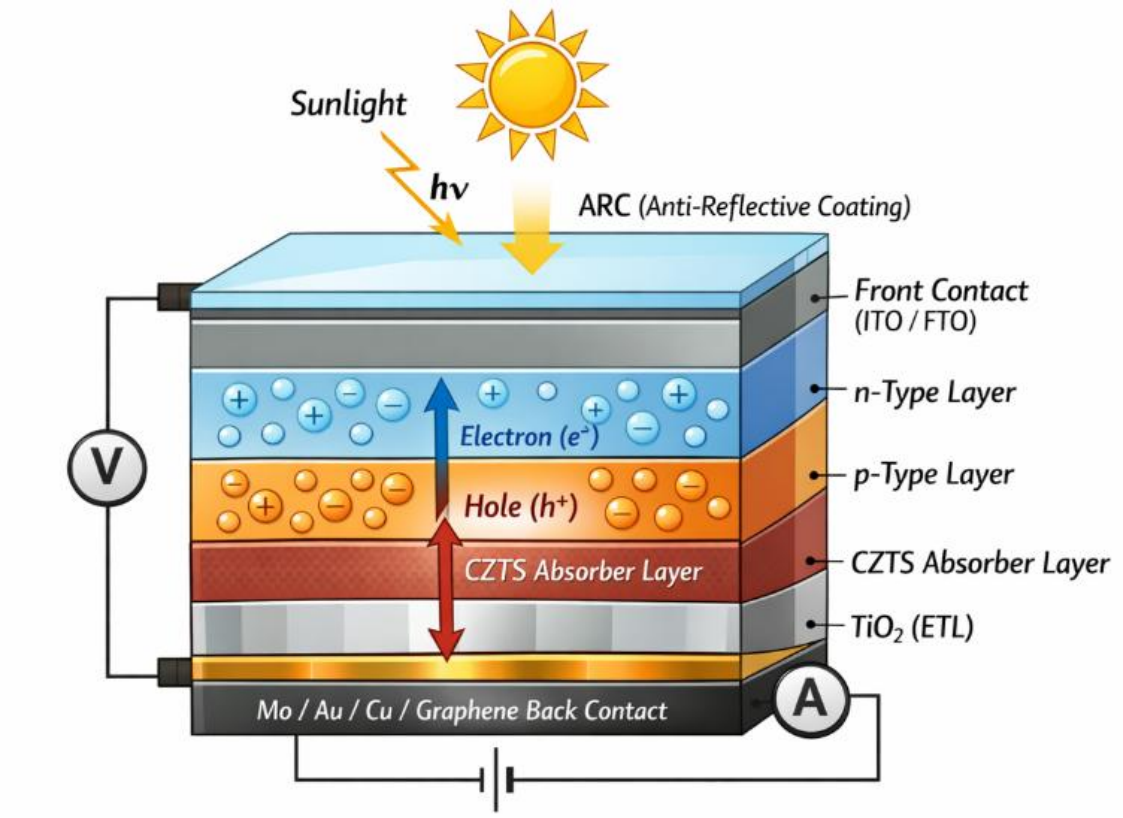

Figure 1: Schematic diagram of multilayer solar cell structure

This general model was modified to various models with the aim of examining the effects of differences in material and structural variables on the performance of a device. A better insight into the efficiency trends and mechanisms of losses might be gained by changing one factor at a time.

In Model 1, a traditional silicon structure was envisaged with n-type and p-type silicon layers. The primary emphasis of the study was on the impact of modification in the layer thickness and operating temperature on the overall efficiency of the device.

In Model 2, a lead free perovskite was used as a design material where the absorber layer is $CsSnI_3$. NiOx was chosen as the hole transport layer and ZnO and SnO_2 were chosen as electron transport layers. This arrangement contributed to the investigation of the functions of transport layers in charge extraction and recombination character.

In Model 3 a more elaborate lead-free perovskite was designed with $CH_3NH_3SnBr_3$ and $FASnI_3$ as the absorber materials. It used FTO as the front contact and optimized ETL and HTL layers to enhance charge transport.

In general, the step-by-step modeling approach enabled to make a more thorough comparison of various solar cell designs and their performance in various conditions.

2.3 Material Parameters and Input Data

The material parameters of both the layers were chosen with care using literature values, and then altered to reflect realistic conditions of the devices. The most important are bandgap energy, electron affinity, carrier mobility, doping concentration, and layer thickness.

Table 1: Electrical and Optical Parameters of Device Layers

Material	Bandgap (eV)	Electron Affinity (eV)	Mobility (cm^2/Vs)	Doping (cm^{-3})	Thickness (nm)
FTO	3.5	4	20	1×10^{19}	500
TiO_2	3.2	4.2	50	1×10^{18}	Variable
ZnO	3.3	4.2	100	1×10^{18}	Variable

Material	Bandgap (eV)	Electron Affinity (eV)	Mobility (cm^2/Vs)	Doping (cm^{-3})	Thickness (nm)
SnO_2	3.6	4.5	50	1×10^{18}	Variable
$CH_3NH_3SnBr_3$	1.3–1.4	4.3	15–20	1×10^{16}	Variable
$FASnI_3$	1.4	4.4	20	1×10^{16}	Variable
Spiro-OMeTAD	3	5.2	5	1×10^{18}	Variable

These values are important in determining carrier transport characteristics, recombination losses and overall photovoltaic performance.

2.4 Simulation Conditions

Each of the simulations was conducted in normal test conditions so that there would be a consistency and different models could be compared. The solar spectrum was AM 1.5G with an intensity of 1000 W/m 2, which is the normal condition on earth. The temperature change was carried out between 280K and 380K to investigate the thermal impacts on the workings of the device. Boundary conditions like contact properties, recombination velocities were fixed unless otherwise.

Table 2: Simulation Conditions and Boundary Parameters

Parameter	Value
Illumination	AM 1.5G
Intensity	1000 W/m^2
Temperature Range	280–380 K
Simulation Mode	Steady-state
Recombination	SRH + Radiative + Auger
Contacts	Ohmic

2.5 Performance Evaluation Parameters

On standard photovoltaic parameters such as open-circuit voltage (Voc), short-circuit current density (Jsc), fill factor (FF) and power conversion efficiency (η) were used to evaluate the performance of the solar cell devices.

The fill factor is defined as:

$$FF = \frac{V_{mp} \times J_{mp}}{V_{oc} \times J_{sc}}$$

The efficiency of the solar cell is calculated as:

$$\eta = \frac{V_{oc} \times J_{sc} \times FF}{P_{in}} \times 100$$

where P_{in}represents the incident solar power density.

These parameters were obtained on basis of simulated JV characteristics and compared against all the models.

2.6 Model-Wise Simulation Strategy

The multi-model simulation technique was used to estimate the impact of various variables on device functionality in a systematic manner.

In Model 1, optimization of silicon-based devices in terms of emitter and absorber thickness variation and temperature analysis was the point of concern. It was done to investigate how the structural parameters impact the carrier generation, recombination, and efficiency.

Model 2 made use of a lead-free perovskite absorber (CsSnI 3) to examine the effects of transport layers. NiOx served as HTL, and ZnO and SnO 2 served as ETLs. The variation in the thickness of these layers was done to reduce the rate of recombination to increase the rate of charge extraction.

An advanced perovskite structure was applied in Model 3 made of CH 3 NH 3 SnBr 3 / FASnI 3 absorber. The structure consisted of FTO as the front contact, TiO 2 as ETL and Spiro-OMeTAD as HTL. These were aimed at maximizing the thickness of the layer, enhancing charge conduction and minimizing recombination losses.

This is a model-driven solution that offers a complete insight of the material choice, the structure of the device, and optimization of the performance.

2.7 Workflow of Simulation

The general simulation process that was used in this study is shown below:

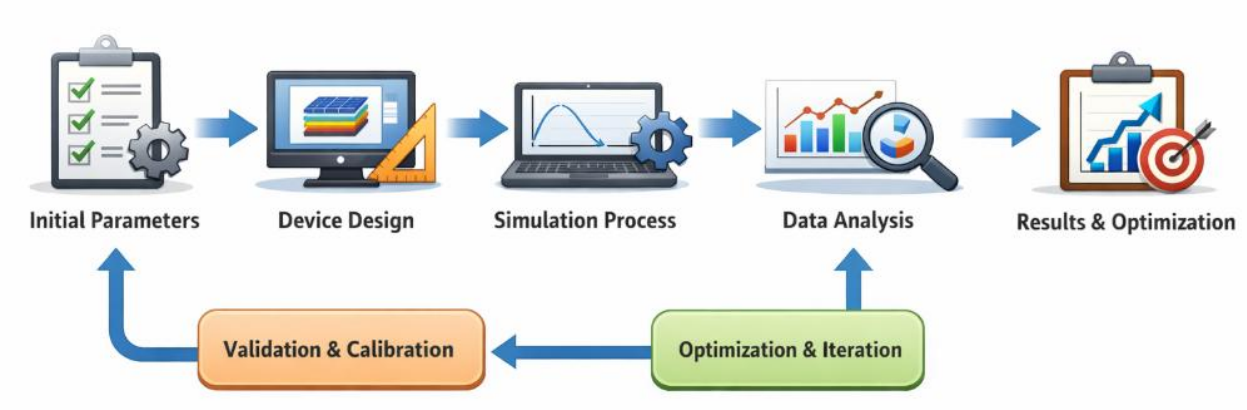

Figure 2: Simulation Workflow Diagram

The workflow starts with the definition of material parameters including bandgap, mobility and doping concentration. This is succeeded by the creation of the multilayer device structure in SCAPS-1D environment. The structure is then defined and simulations are then run with

given illumination and boundary conditions to achieve output characteristics of JV curves, quantum efficiency (QE) and recombination profiles.

The results obtained are pulled out and analyzed to give major parameters of performance such as Voc, Jsc, fill factor, and efficiency. According to these findings, the process of iterative optimization is used to achieve a material property and layer thickness changes. This rules-based workflow facilitates proper evaluation of the performance and enhances the trust and repeatability of the simulation outputs.

3. RESULTS AND DISCUSSION

3.1 Model 1 – Back Contact and Device Optimization (Silicon Solar Cell)

The silicon-based solar cell performance was studied in the context of the effects of various back contact material and thermal performance. The back contact influences considerably carrier extraction efficiency, recombination processes, and overall device operation because it has an influence on the alignment of the energy bands.

Figure 3 shows the currentvoltage characteristics of the various back contact materials. As is found, high work function metals like gold (Au) and copper (Cu) perform better and have better open-circuit voltage (Voc) and fill factors (FF). Conversely, iron (Fe) and graphene devices exhibit reduced performance of poor band alignment and carrier extraction. The enhanced performance of Au and Cu is explained by the enhanced performance in terms of hole collection and decreased interface recombination losses.

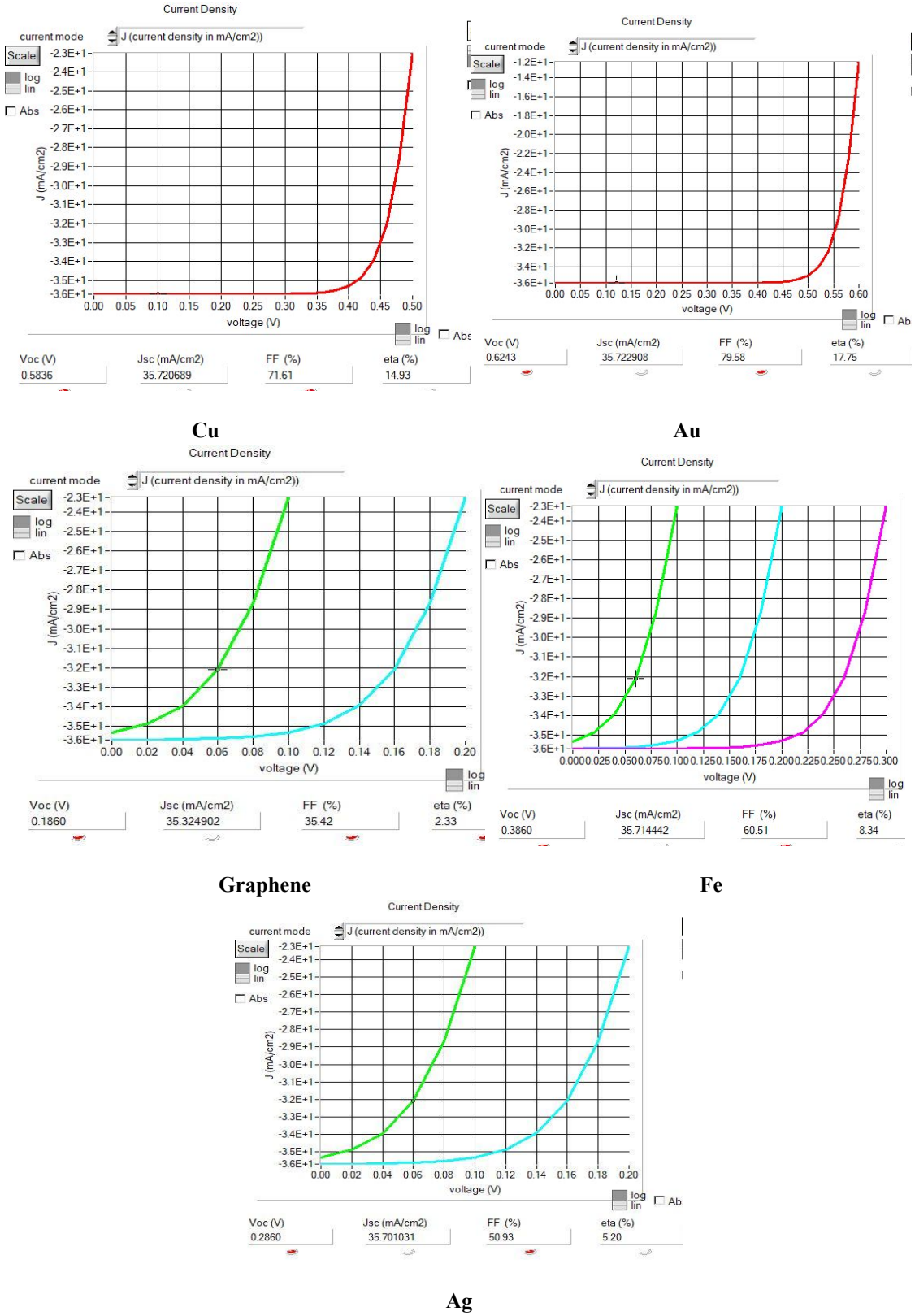

Figure 3: J–V characteristics for different back contacts (Au, Cu, Ag, Fe, Graphene)

Further examination of the physics of the device was done through recombination behavior and presented in Figure 4. The findings show that Shockley-Read-Hall (SRH) recombination prevails in the performance of the device. Graphene and Fe-based were found to have a high recombination current whereas Au and Cu contacts suppress recombination effectively. This decrease in recombination has a direct positive impact on efficiency.

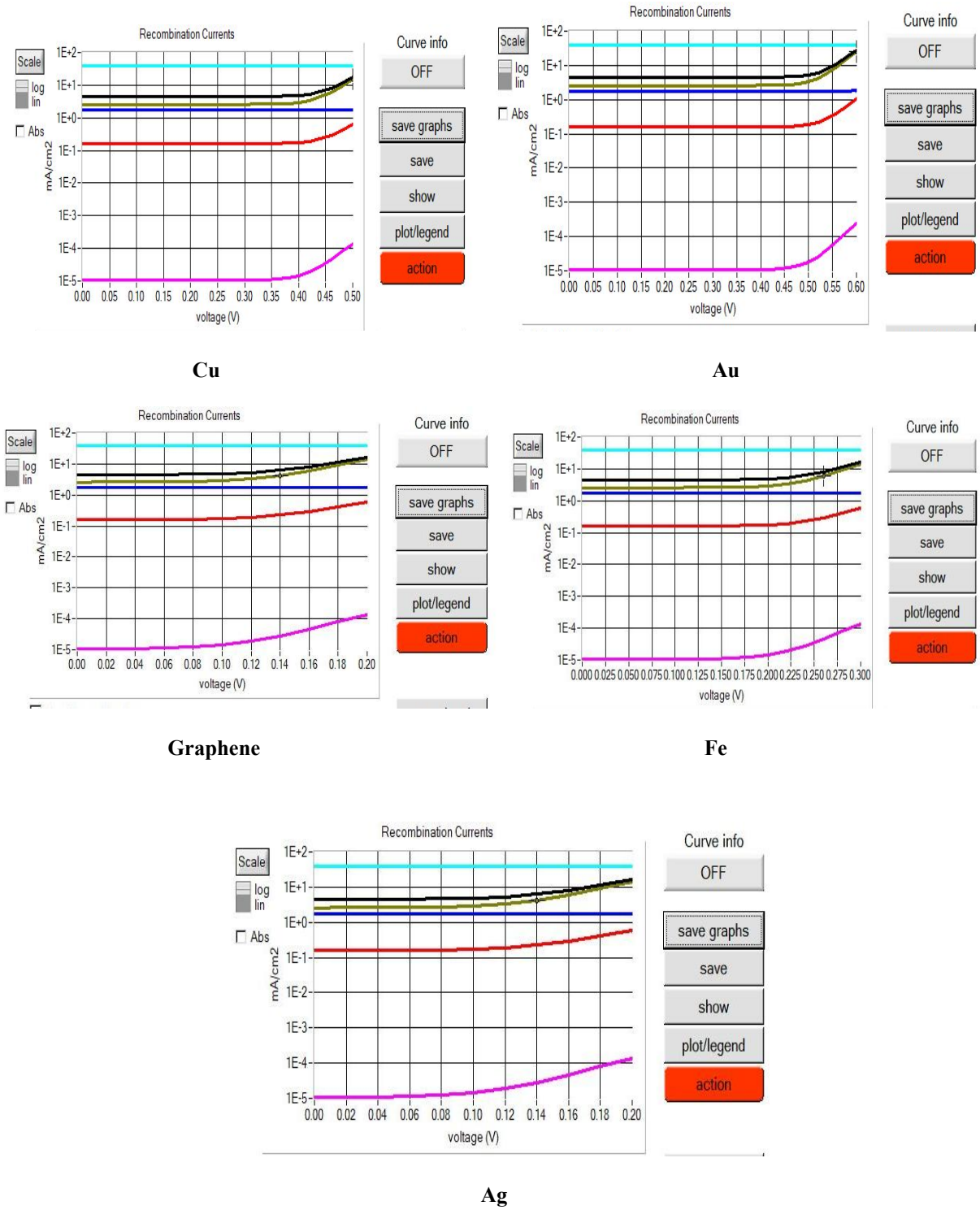

Figure 4: Recombination current comparison for best (Au/Cu/Ag/Graphene/Fe) contacts

Figure 5. shows the quantum efficiency spectra in the device, which is used to show the optical performance of the device. The values of the QE are found to be large in the visible spectrum (~90 - 100%), which implies that the photons are well absorbed and carriers are generated. Optimized back contacts are found on devices that exhibit enhanced carrier collection especially in the short wavelength range.

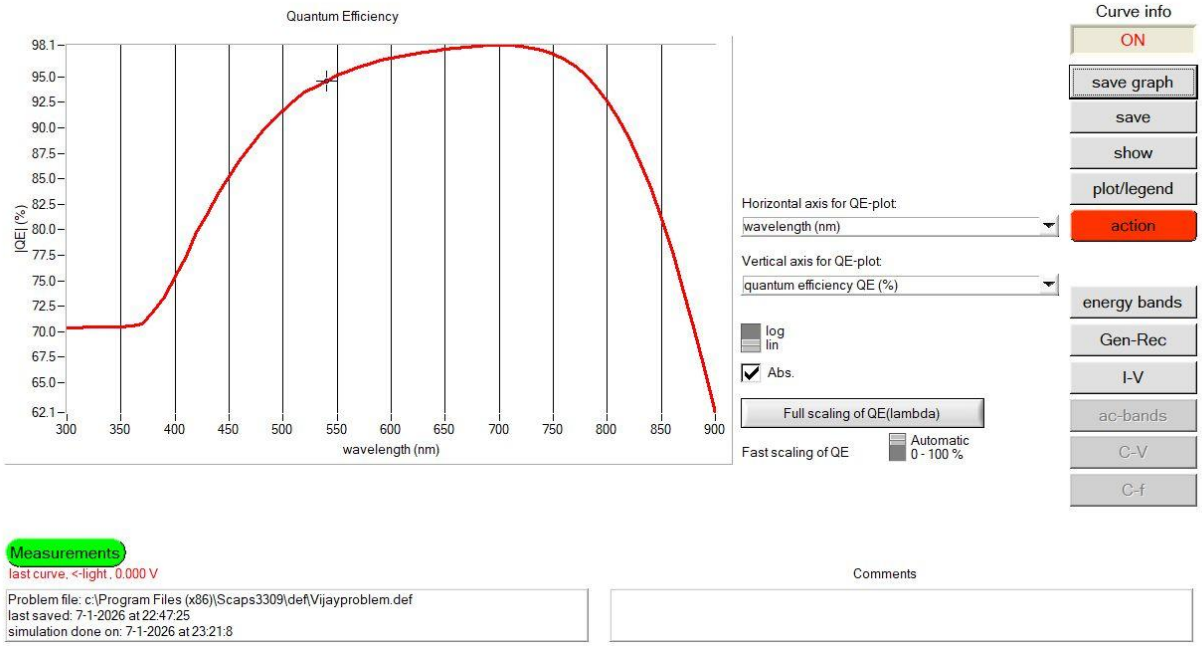

10QE

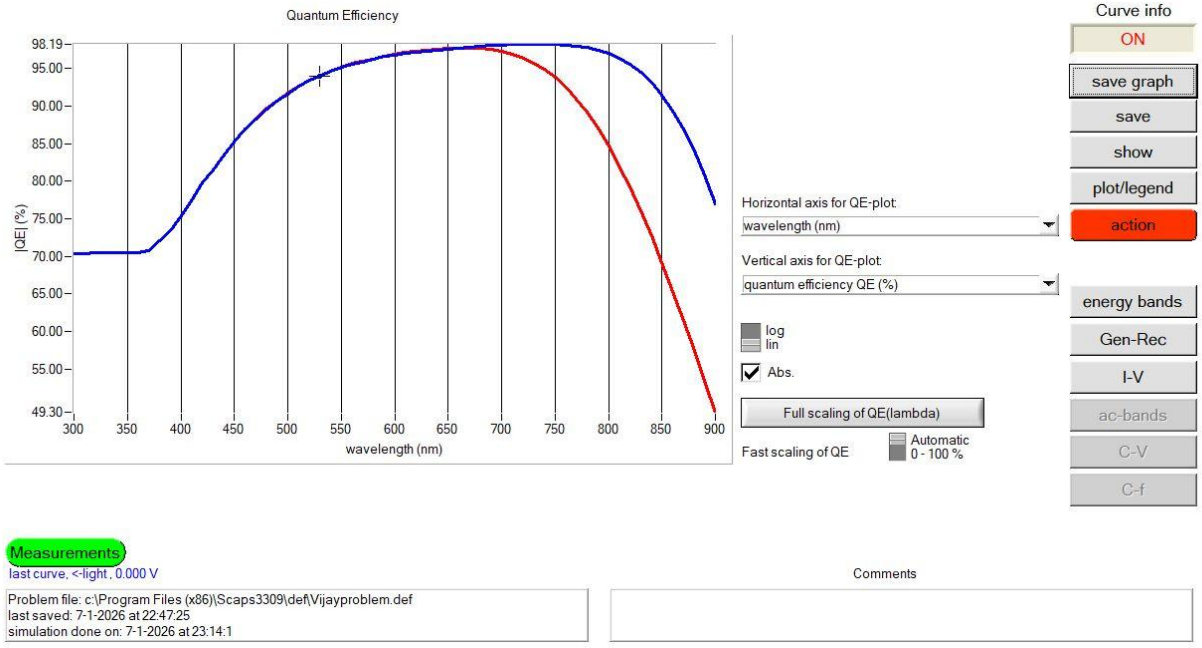

28QE

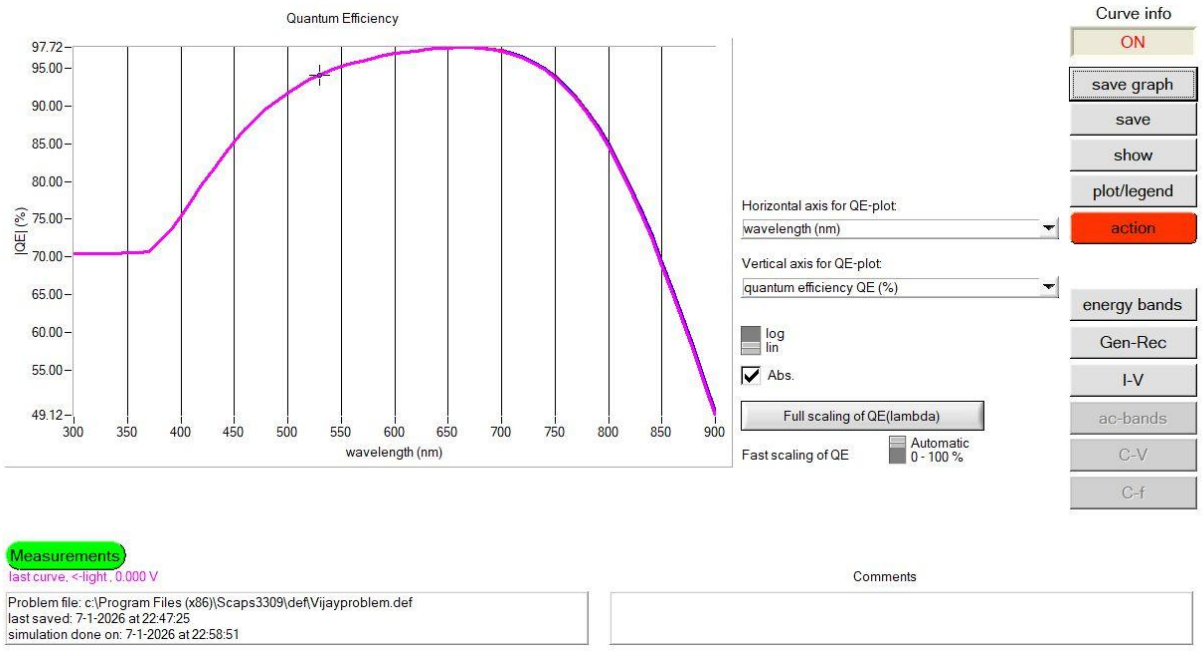
Quantum Efficiency
97.72
95.00
90.00
85.00
80.00
75.00
70.00
65.00
60.00
55.00
49.12
|QE| (%)
300 350 400 450 500 550 600 650 700 750 800 850 900
wavelength (nm)
Curve info
ON
save graph
save
show
plot/legend
action
Horizontal axis for QE-plot:
wavelength (nm)
Vertical axis for QE-plot:
quantum efficiency QE (%)
log
lin
Abs.
Full scaling of QE(lambda)
Fast scaling of QE
Automatic
0 - 100 %
energy bands
Gen-Rec
I-V
ac-bands
C-V
C-f
Measurements
last curve, <-light , 0.000 V
Comments
Problem file: c:\Program Files (x86)\Scaps3309\def\Vijayproblem.def
last saved: 7-1-2026 at 22:47:25
simulation done on: 7-1-2026 at 22:58:51

100QE

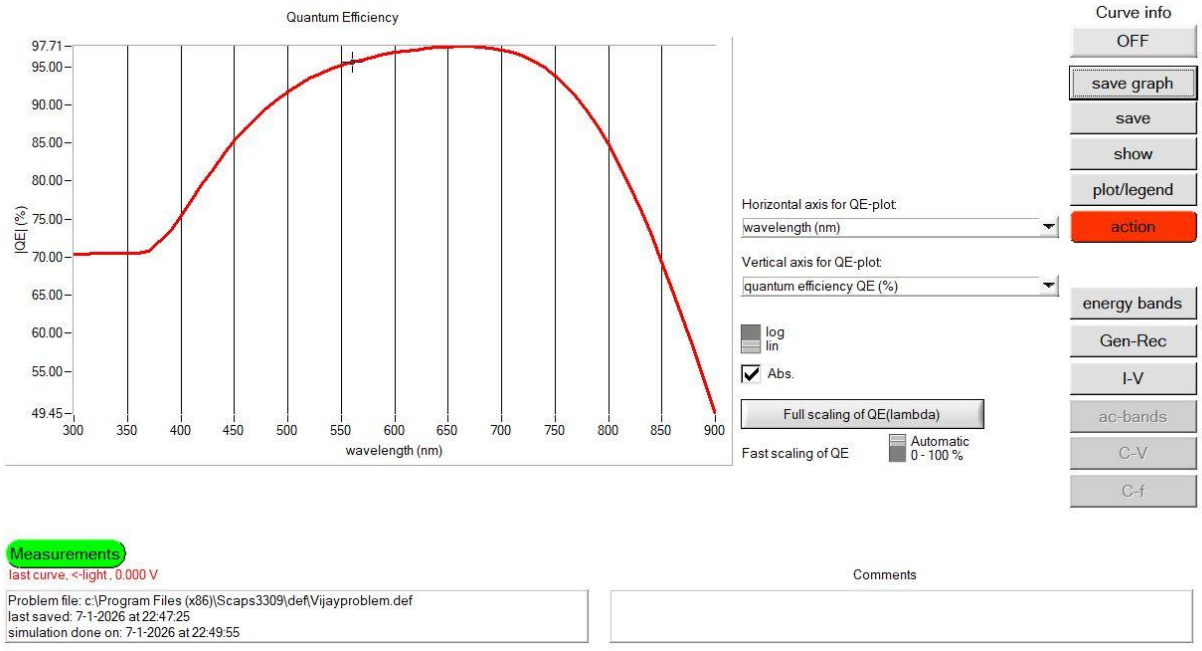
Quantum Efficiency
97.71
95.00
90.00
85.00
80.00
75.00
70.00
65.00
60.00
55.00
49.45
|QE| (%)
300 350 400 450 500 550 600 650 700 750 800 850 900
wavelength (nm)
Curve info
OFF
save graph
save
show
plot/legend
action
Horizontal axis for QE-plot:
wavelength (nm)
Vertical axis for QE-plot:
quantum efficiency QE (%)
log
lin
Abs.
Full scaling of QE(lambda)
Fast scaling of QE
Automatic
0 - 100 %
energy bands
Gen-Rec
I-V
ac-bands
C-V
C-f
Measurements
last curve, <-light , 0.000 V
Comments
Problem file: c:\Program Files (x86)\Scaps3309\def\Vijayproblem.def
last saved: 7-1-2026 at 22:47:25
simulation done on: 7-1-2026 at 22:49:55

300QE

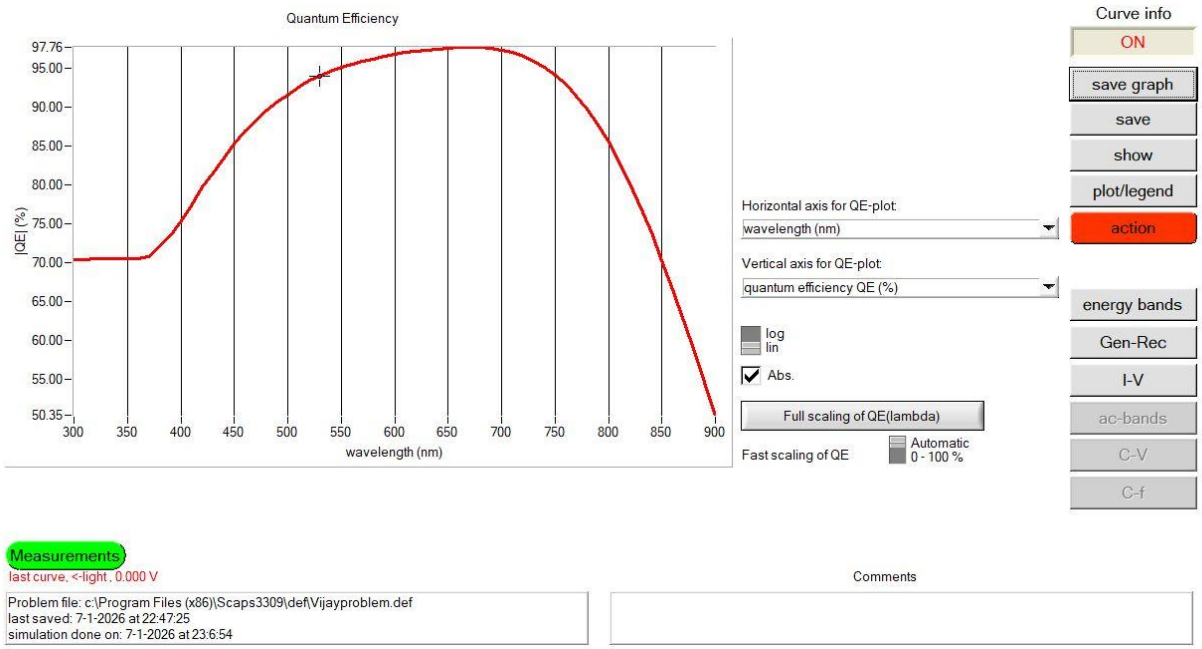

500QE

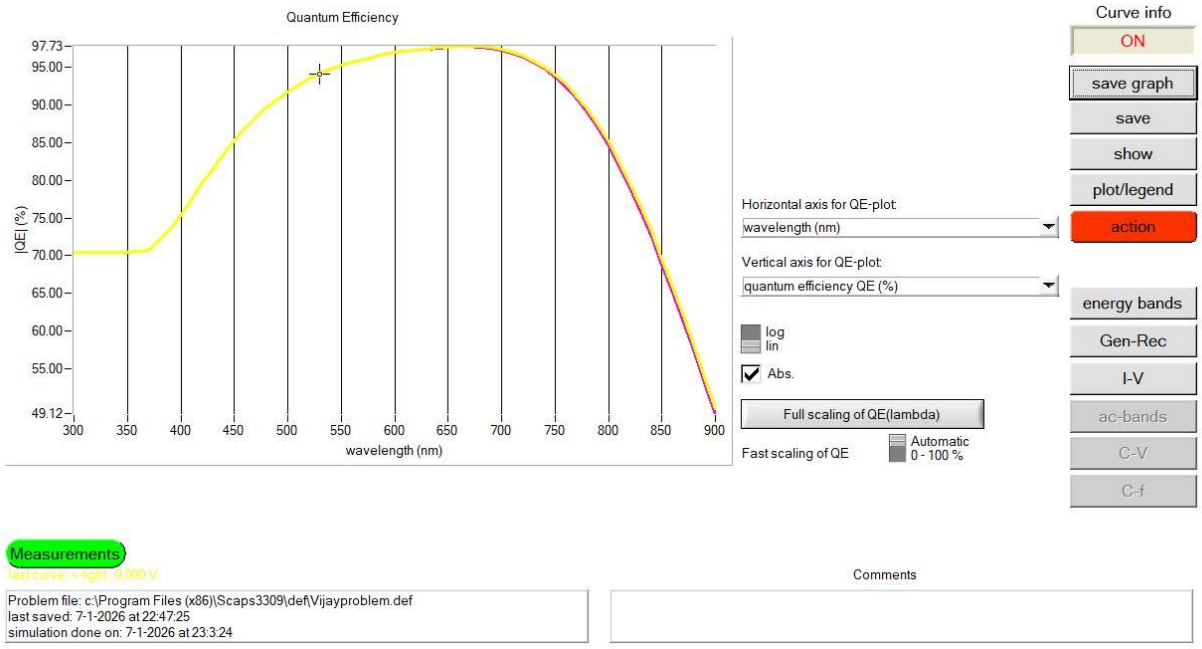

900QE

Figure 5: Quantum Efficiency (QE) spectra for different back contacts

"The impact of temperature on the working of the devices is depicted in Figure 6. On increasing temperatures, there is a strong reduction in the open-circuit voltage (Voc) and a slight increase in the short-circuit current density (Jsc)". The fall in Voc is primarily because of the narrowing of the bandgaps and higher intrinsic carrier concentration that increases recombination. Accordingly, the efficiency declines with the rise in temperature.

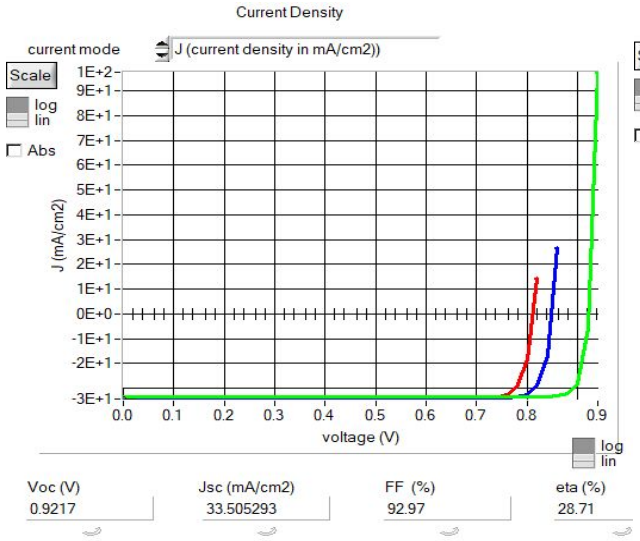
Current Density
current mode
J (current density in mA/cm2))
Scale
log
lin
Abs
J (mA/cm2)
voltage (V)
Voc (V)
0.9217
Jsc (mA/cm2)
33.505293
FF (%)
92.97
eta (%)
28.71

140

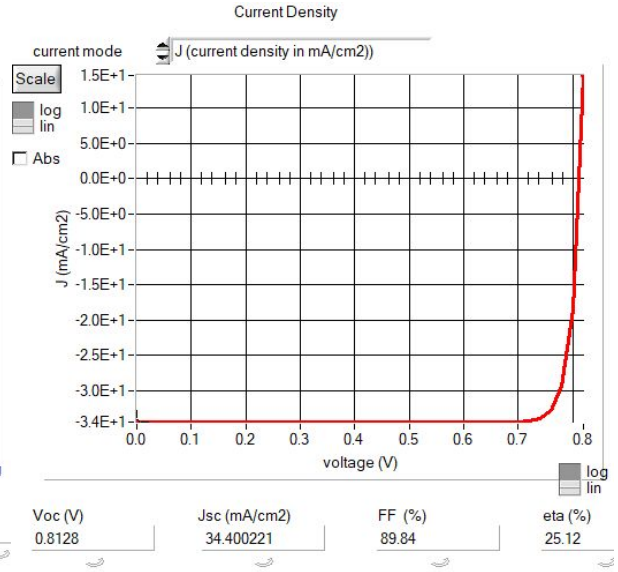
Current Density
current mode
J (current density in mA/cm2))
Scale
log
lin
Abs
J (mA/cm2)
voltage (V)
Voc (V)
0.8128
Jsc (mA/cm2)
34.400221
FF (%)
89.84
eta (%)
25.12

200

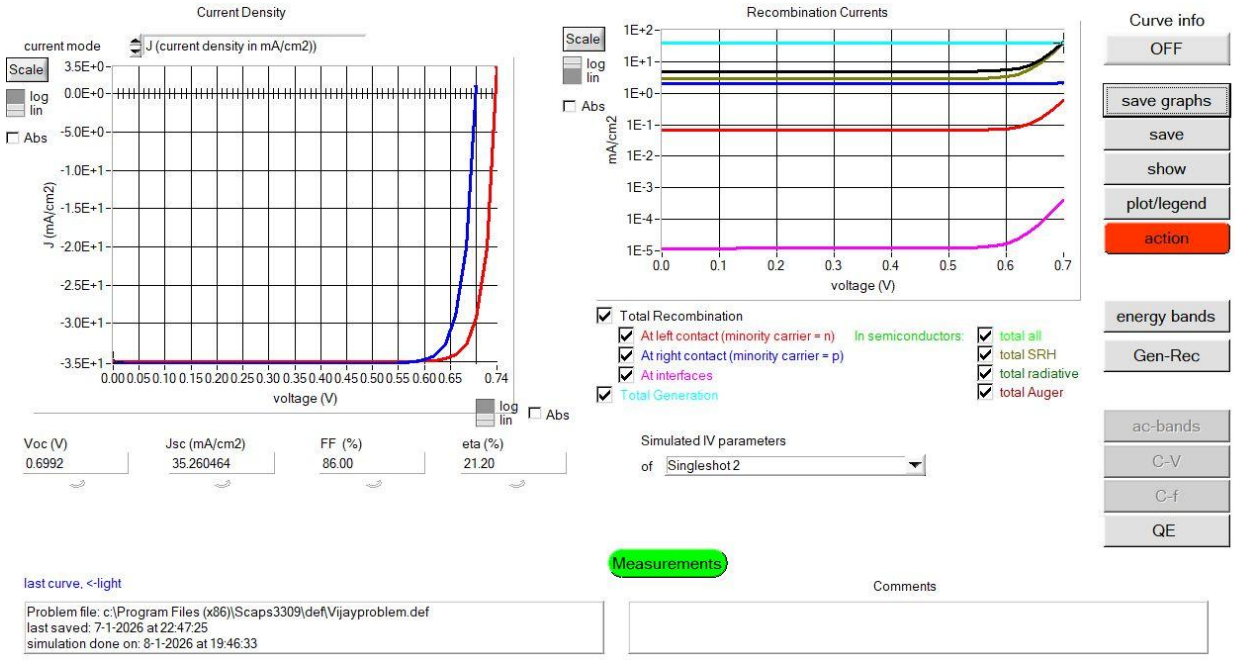
Current Density
current mode
J (current density in mA/cm2))
Scale
log
lin
Abs
J (mA/cm2)
voltage (V)
Voc (V)
0.6992
Jsc (mA/cm2)
35.260464
FF (%)
86.00
eta (%)
21.20
Recombination Currents
mA/cm2
voltage (V)
Total Recombination
At left contact (minority carrier = n)
At right contact (minority carrier = p)
At interfaces
Total Generation
In semiconductors:
total all
total SRH
total radiative
total Auger
Simulated IV parameters
of
Singleshot 2
Curve info
OFF
save graphs
save
show
plot/legend
action
energy bands
Gen-Rec
ac-bands
C-V
C-f
QE
Measurements
last curve, <-light
Comments
Problem file: c:\Program Files (x86)\Scaps3309\def\Vijayproblem.def
last saved: 7-1-2026 at 22:47:25
simulation done on: 8-1-2026 at 19:46:33

260

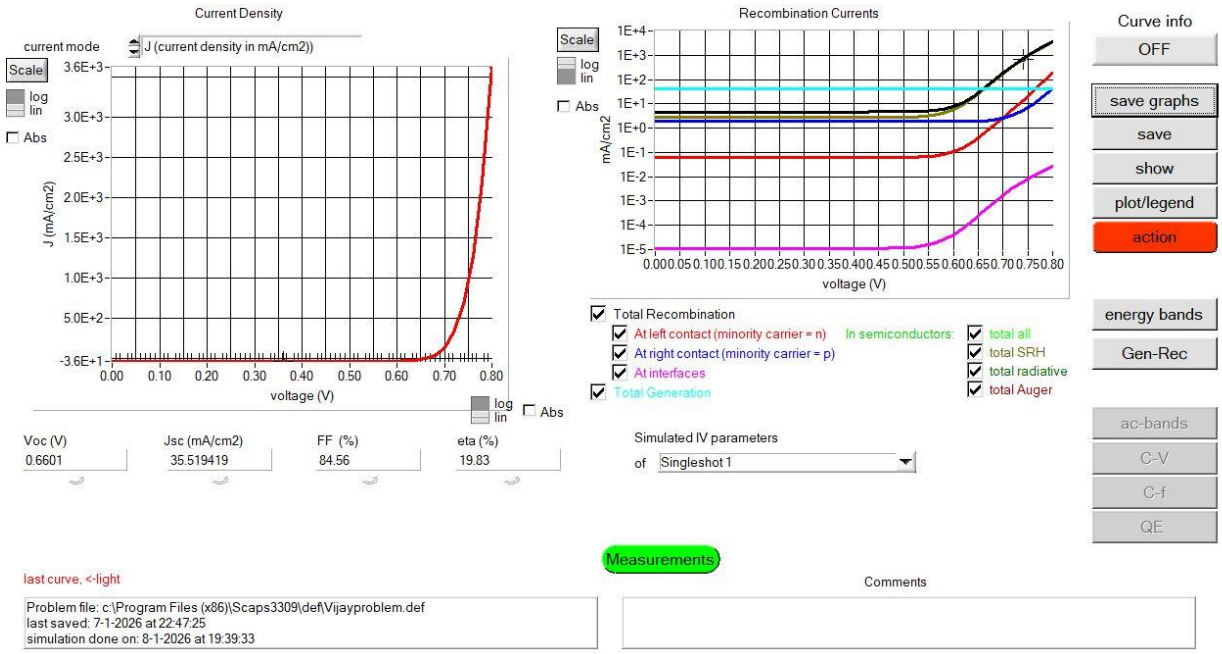
Current Density
current mode
J (current density in mA/cm2))
Scale
log
lin
Abs
J (mA/cm2)
voltage (V)
Recombination Currents
mA/cm2
Curve info
OFF
save graphs
save
show
plot/legend
action
energy bands
Gen-Rec
ac-bands
C-V
C-f
QE
Total Recombination
At left contact (minority carrier = n)
At right contact (minority carrier = p)
At interfaces
Total Generation
In semiconductors:
total all
total SRH
total radiative
total Auger
Voc (V)
0.6601
Jsc (mA/cm2)
35.519419
FF (%)
84.56
eta (%)
19.83
Simulated IV parameters
of
Singleshot 1
Measurements
last curve, <-light
Comments
Problem file: c:\Program Files (x86)\Scaps3309\def\Vijayproblem.def
last saved: 7-1-2026 at 22:47:25
simulation done on: 8-1-2026 at 19:39:33

280

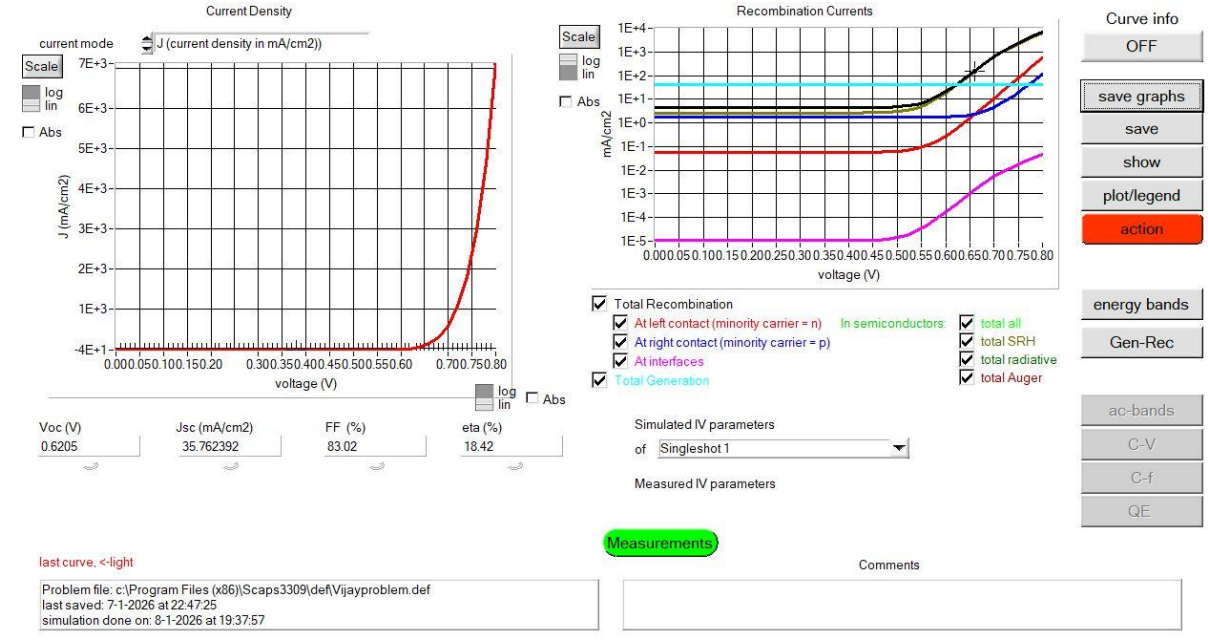
Current Density
current mode
J (current density in mA/cm2))
Scale
log
lin
Abs
J (mA/cm2)
voltage (V)
Recombination Currents
mA/cm2
Curve info
OFF
save graphs
save
show
plot/legend
action
energy bands
Gen-Rec
ac-bands
C-V
C-f
QE
Total Recombination
At left contact (minority carrier = n)
At right contact (minority carrier = p)
At interfaces
Total Generation
In semiconductors:
total all
total SRH
total radiative
total Auger
Voc (V)
0.6205
Jsc (mA/cm2)
35.762392
FF (%)
83.02
eta (%)
18.42
Simulated IV parameters
of
Singleshot 1
Measured IV parameters
Measurements
last curve, <-light
Comments
Problem file: c:\Program Files (x86)\Scaps3309\def\Vijayproblem.def
last saved: 7-1-2026 at 22:47:25
simulation done on: 8-1-2026 at 19:37:57

300

P-SI SOLAR SELL

Figure 6: Temperature dependent J–V characteristics

The overall performance parameters corresponding to different conditions are summarized in Table 3.

Table 3: Summary of Model 1 Performance Parameters

Parameter	Best Case (Au/Cu)	Worst Case (Graphene/Fe)	Temperature Effect
Voc (V)	0.62 – 0.66	~0.60 or lower	Decreases with temperature
Jsc (mA/cm²)	~37.45	~36–37	Slight increase
FF (%)	~83	~75–80	Decreases
Efficiency (%)	~19.33	~17–18	Decreases

The findings discussed in Table 3.1 affirm that Au and Cu back contacts have the most efficiency, and graphene has the worst performance because of increased recombination losses. Comprehensively, the performance of the devices is highly dependent on the choice of back contact and temperature change.

The interpretation shows that effective back contact engineering can be of great use in improving the performance of the device by diminishing the recombination and maximizing the carrier extraction. The efficiency of the optimized silicon solar cell is recorded to be at about 19.33 percent with temperature increase having an adverse influence on the efficiency owing to increase in recombination.

3.2 Model 2 Lead-Free Solar Cell (Transport Layer and Absorber Engineering)

The second model examines the efficiency of a lead-free perovskite solar cell based on the analysis of the absorber properties, transport layers, and recombination behavior. The purpose of this model is to assess the fact that lead-free material can possibly offer a similar performance to silicon-based devices.

The JV characteristics in various device configurations are expressed in Figure 7. It is seen that the short-circuit current density (Jsc) is rather high, and it is a sign of intense optical absorption. Here however, the fill factor (FF) is

greatly smaller, which results in skewed J V curves. This behavior implies that there are high series resistance and inefficient charge transport in the device.

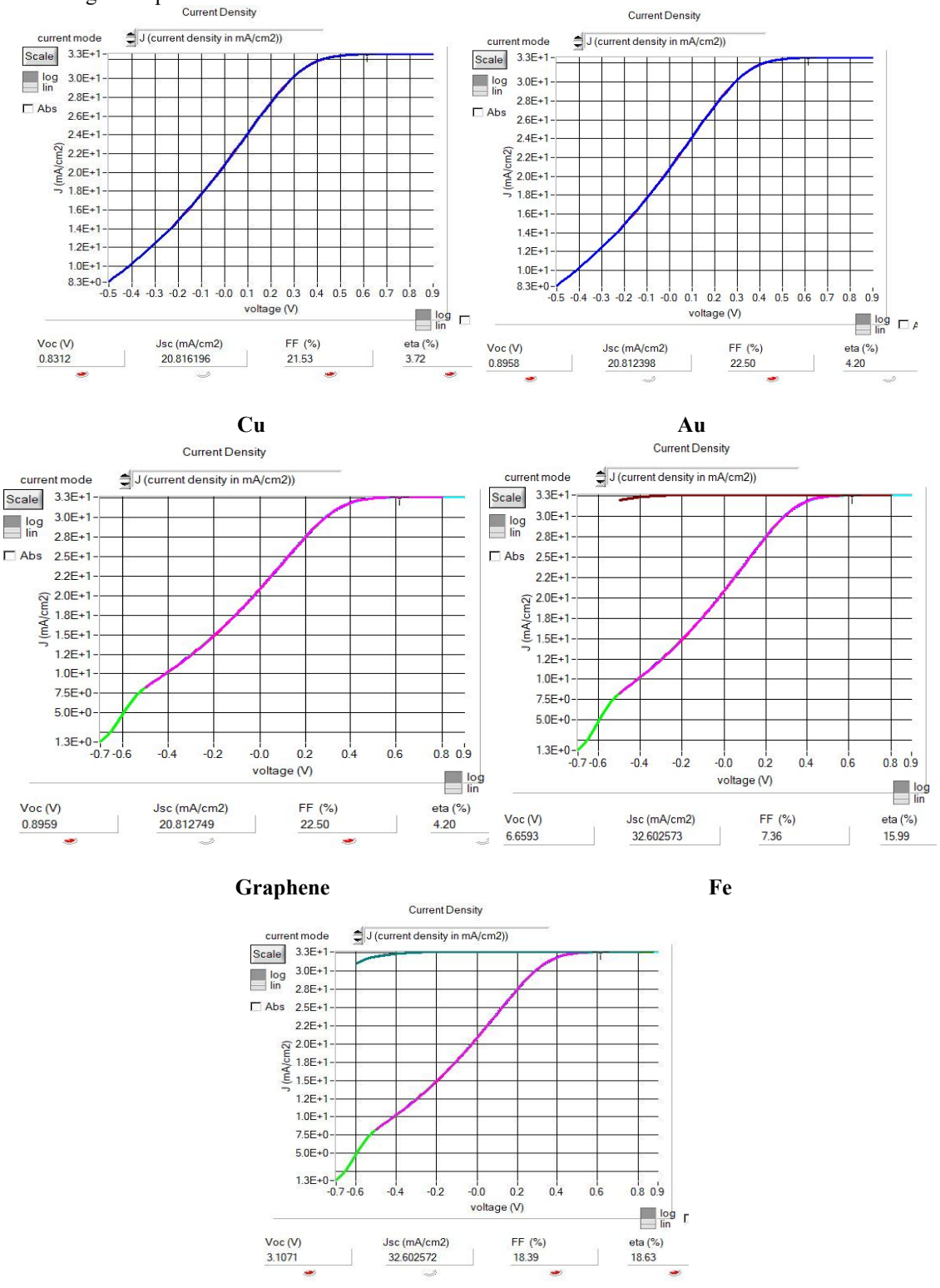

Figure 7: J–V characteristics for different device cases (lead-free model)

Figure 8: gives the recombination properties. It can be clearly seen that the recombination is much greater than in Model 1 and the bulk SRH recombination prevails with the loss mechanisms. This due to the high defect density with the lead-free absorber means that the carrier lifetime is reduced and recombination losses are high causing a limited device performance.

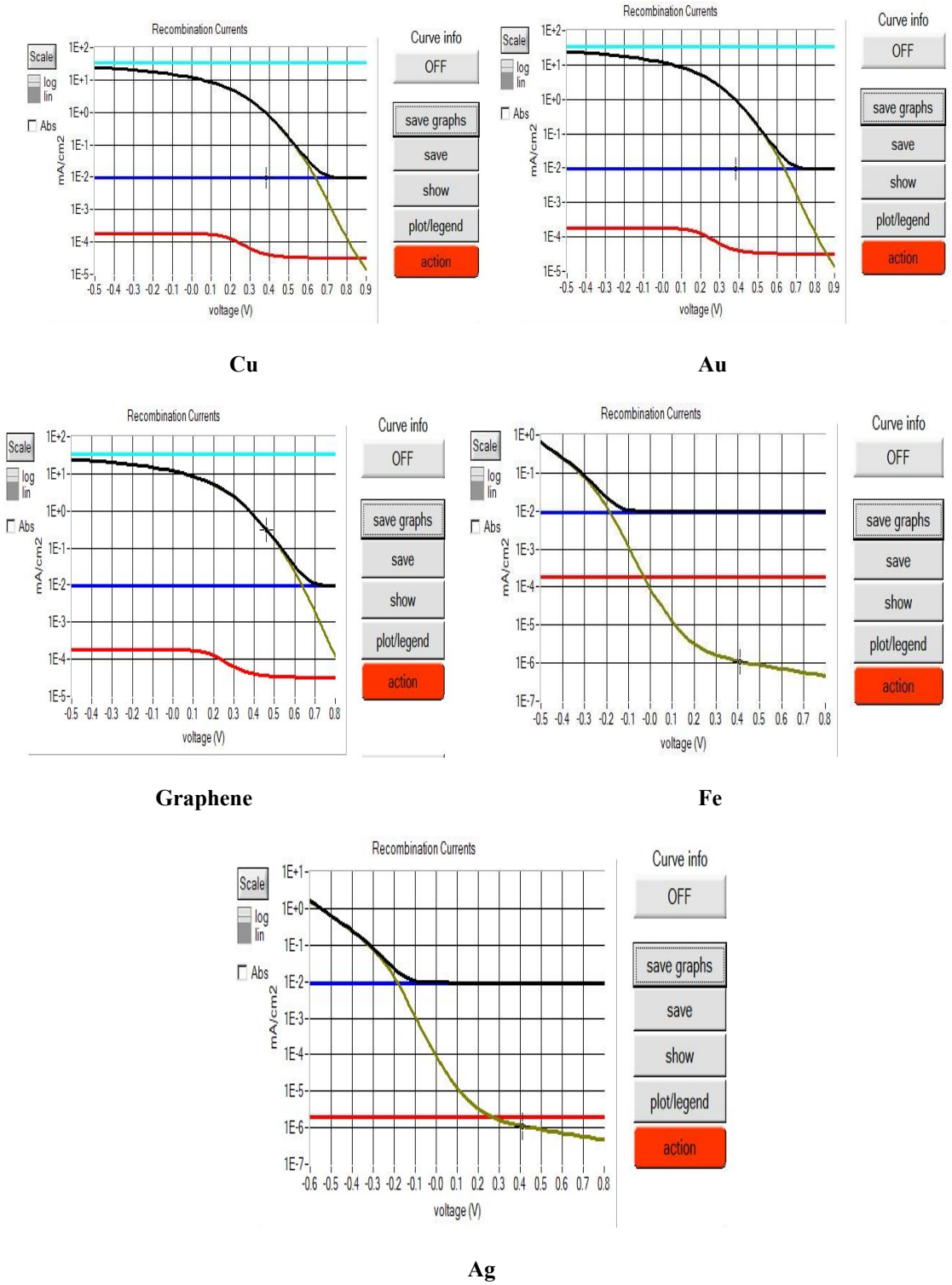

Figure 8: Recombination current analysis (bulk vs total recombination)

The extracted performance parameters are summarized in Table 4.

Table 4: Summary of Model 2 Performance Parameters

Case	Voc (V)	Jsc (mA/cm²)	FF (%)	Efficiency (%)
Case 1	0.659	32.6	7.36	15.99
Case 2	0.31	32.6	18.39	18.63
Case 3	0.831	20.81	21.53	3.72
Case 4	0.895	20.81	22.5	4.2
Case 5	0.895	20.81	22.5	4.2

Table 3.2 results show that relatively high values of current density are obtained but the overall efficiency is low because of very low fill factor and large recombination losses. Such fluctuation of Voc among different cases also speaks of a lack of stability in junction properties and material quality.

The lead-free solar cell has high optical absorption and low electrical performance. Low fill factor and high recombination rates cause severe limitations of efficiency. Thus, material quality, defect passivation and interface engineering still need further optimization to enhance device performance.

3.3 Model 3 Advanced Perovskite Solar Cell ($CH_3NH_3SnBr_3$)

Model 3 is a high-end lead-free perovskite solar cell design, using “CH 3 NH 3 SnBr 3 as an absorber” and in which a multi parameter optimization scheme is used. The analysis involves the variation of absorber thickness, engineering of back contacts, optimization of the transport layer and temperature-sensitivity. The proposed model will enhance charge movement and minimize the recombination losses as well as increase the effectiveness of the device.

3.3.1 Absorber Thickness Optimization

The character of absorber layer thickness on the device performance is concerned with using the J-V characteristic of Figure 9. It is seen that the efficiency and increases with the thickness, first because more photons are absorbed and carriers are generated. Nevertheless, when the thickness is further increased, the efficiency starts to drop because more losses stemming from recombinations in the bulk region occur.

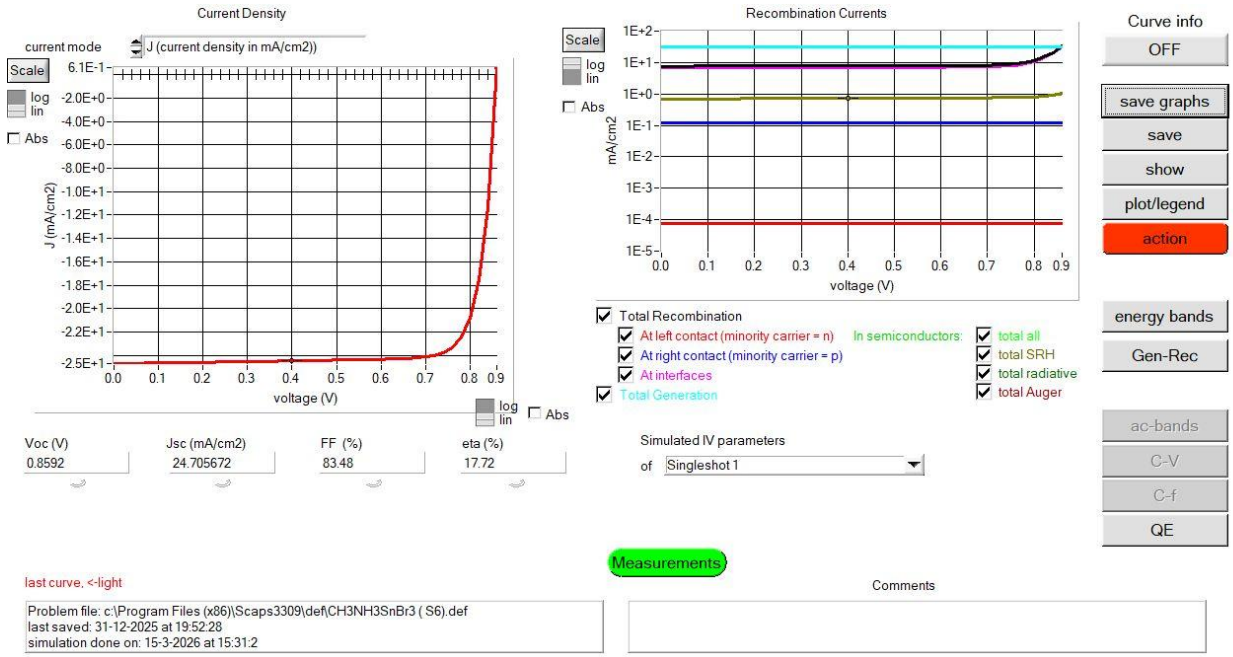

0.3um

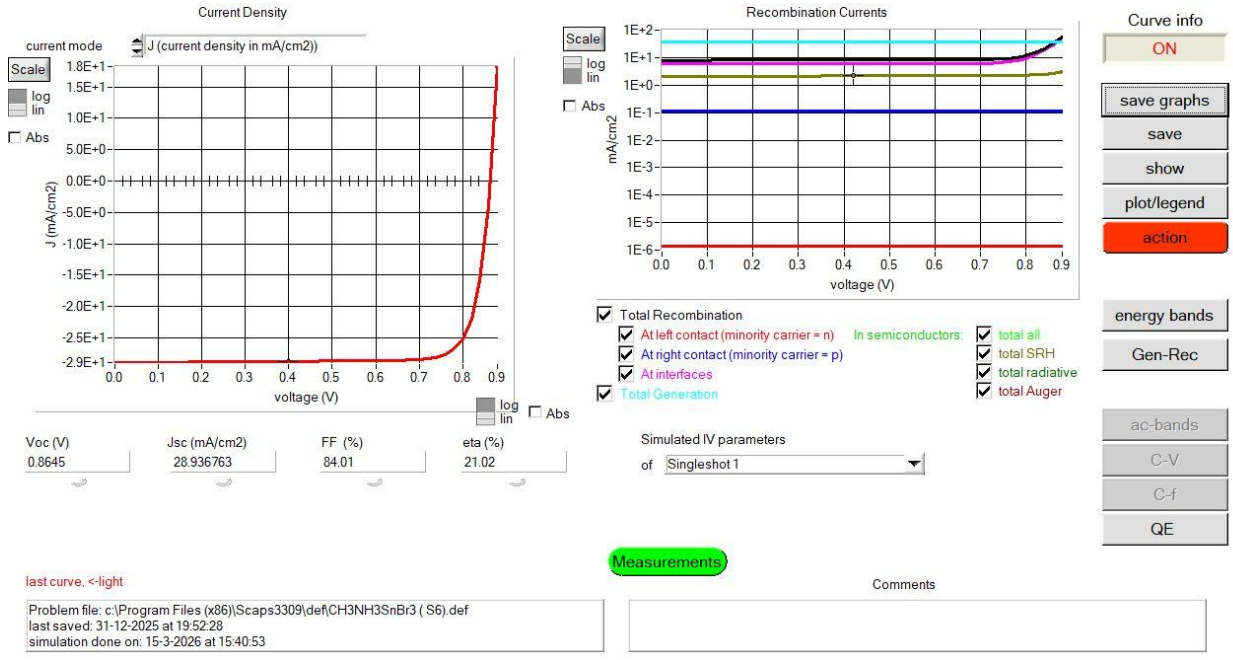
Current Density
current mode
J (current density in mA/cm2))
Scale
log
lin
Abs
J (mA/cm2)
voltage (V)
Recombination Currents
mA/cm2
Total Recombination
At left contact (minority carrier = n)
At right contact (minority carrier = p)
At interfaces
Total Generation
In semiconductors:
total all
total SRH
total radiative
total Auger
Curve info
ON
save graphs
save
show
plot/legend
action
energy bands
Gen-Rec
ac-bands
C-V
C-f
QE
Voc (V)
0.8645
Jsc (mA/cm2)
28.936763
FF (%)
84.01
eta (%)
21.02
Simulated IV parameters
of
Singleshot 1
Measurements
last curve, <-light
Comments
Problem file: c:\Program Files (x86)\Scaps3309\def\CH3NH3SnBr3 (S6).def
last saved: 31-12-2025 at 19:52:28
simulation done on: 15-3-2026 at 15:40:53

0.7um

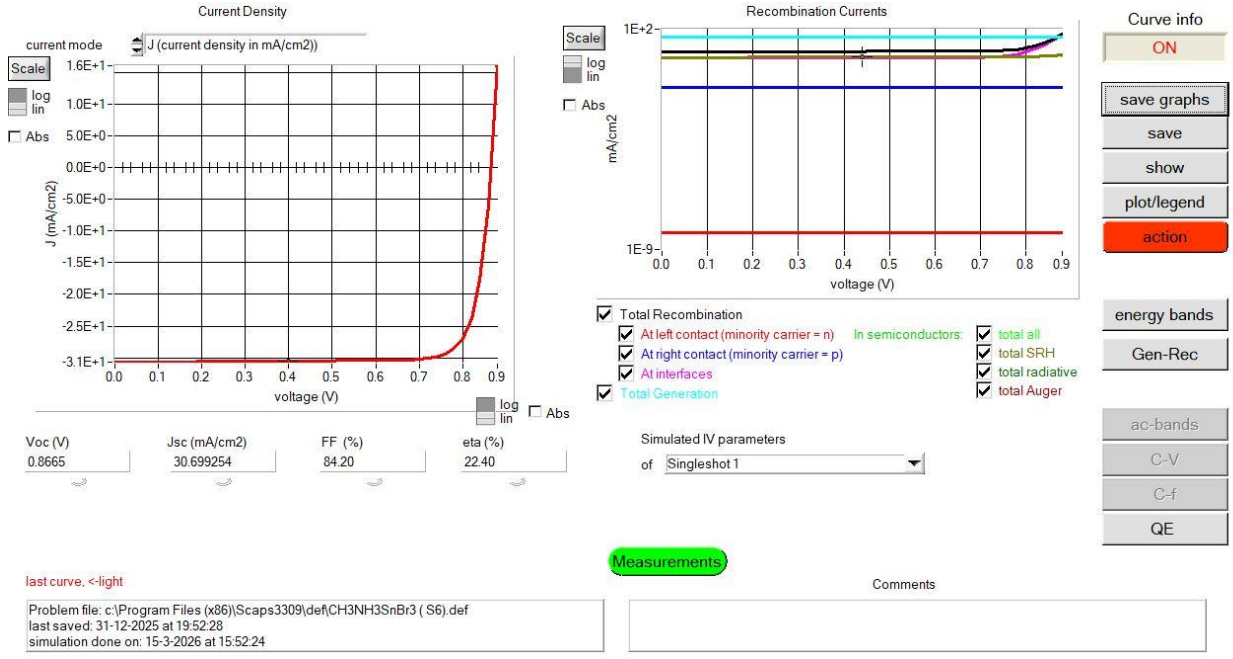
Current Density
current mode
J (current density in mA/cm2))
Scale
log
lin
Abs
J (mA/cm2)
voltage (V)
Recombination Currents
mA/cm2
Total Recombination
At left contact (minority carrier = n)
At right contact (minority carrier = p)
At interfaces
Total Generation
In semiconductors:
total all
total SRH
total radiative
total Auger
Curve info
ON
save graphs
save
show
plot/legend
action
energy bands
Gen-Rec
ac-bands
C-V
C-f
QE
Voc (V)
0.8665
Jsc (mA/cm2)
30.699254
FF (%)
84.20
eta (%)
22.40
Simulated IV parameters
of
Singleshot 1
Measurements
last curve, <-light
Comments
Problem file: c:\Program Files (x86)\Scaps3309\def\CH3NH3SnBr3 (S6).def
last saved: 31-12-2025 at 19:52:28
simulation done on: 15-3-2026 at 15:52:24

1um

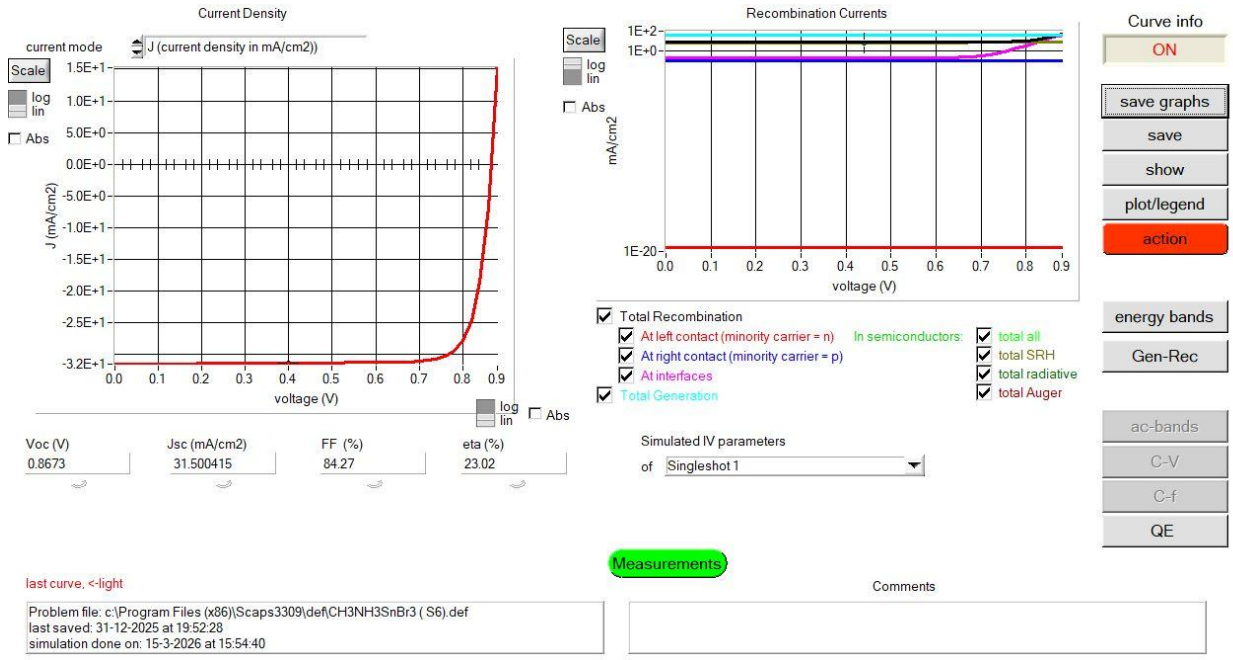

3um

Figure 9: J–V characteristics for absorber thickness variation

Figure 10 shows the corresponding quantum efficiency (QE) spectra. The QE increases in the first range with the thickness because of increased light absorption. Nevertheless, beyond the larger values of thickness, the QE tends to saturate and level off more, showing that recombination losses are at play in the collection of the carriers.

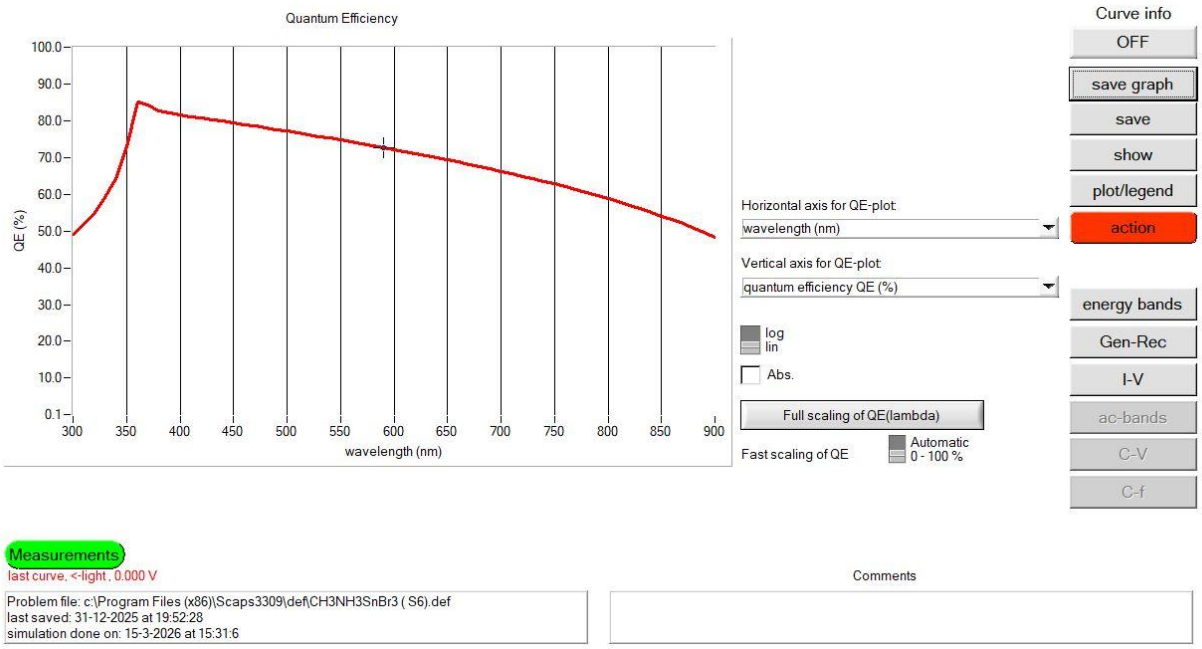

0.3 um Qe

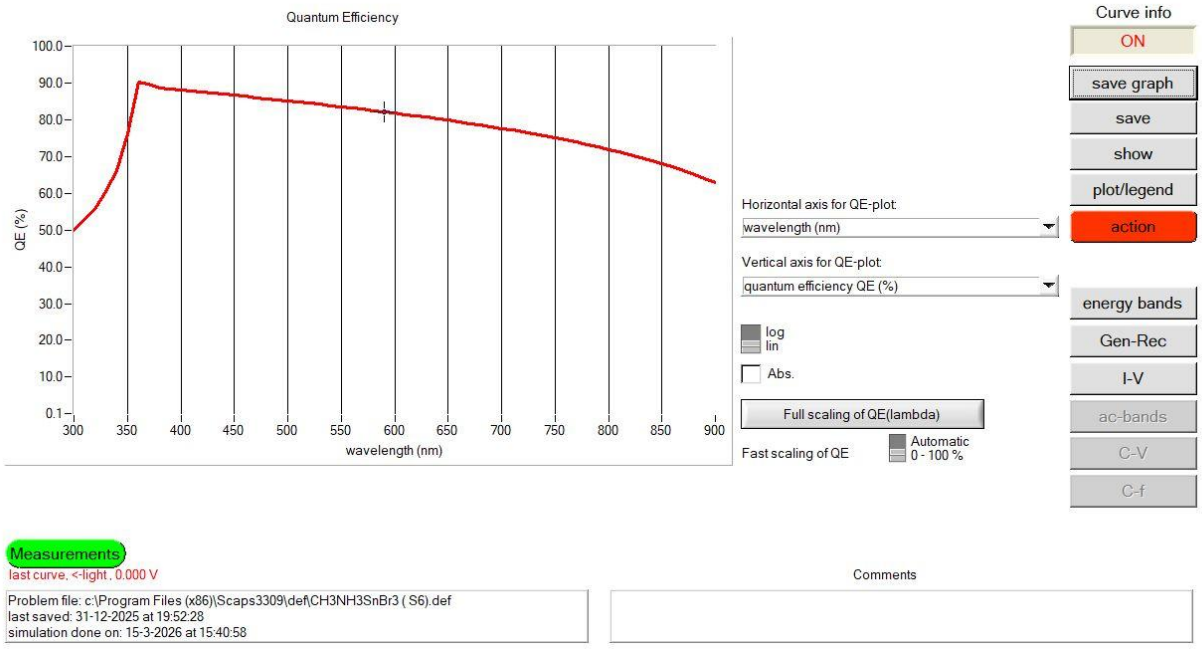

0.06 um Qe

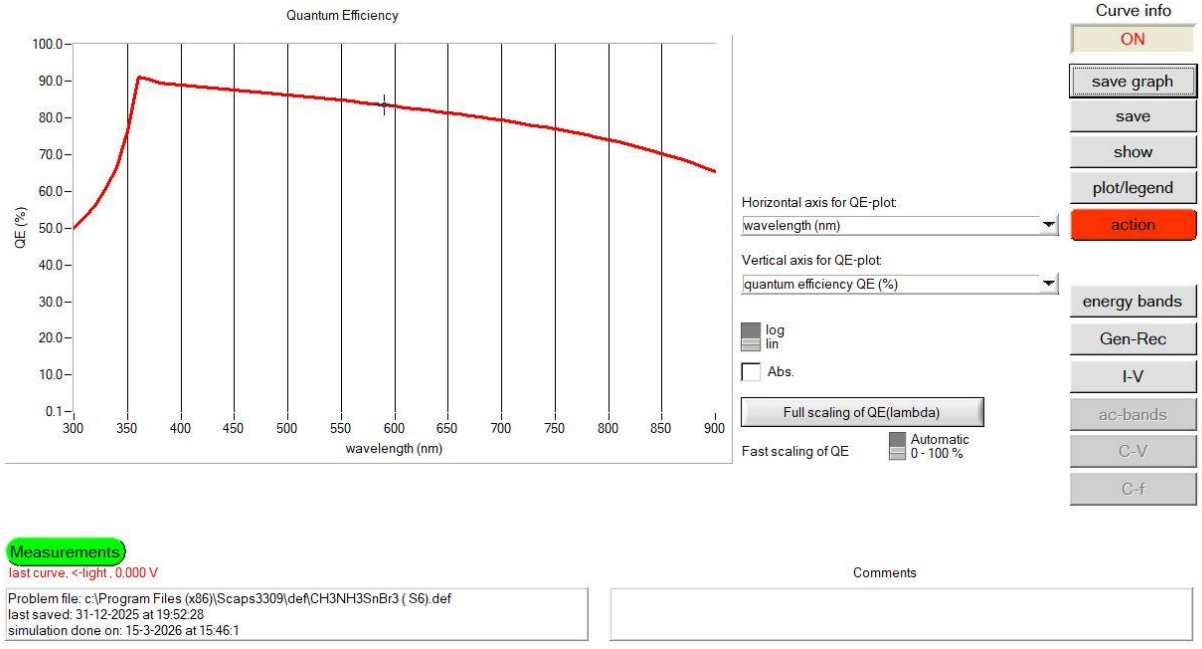

1um Qe

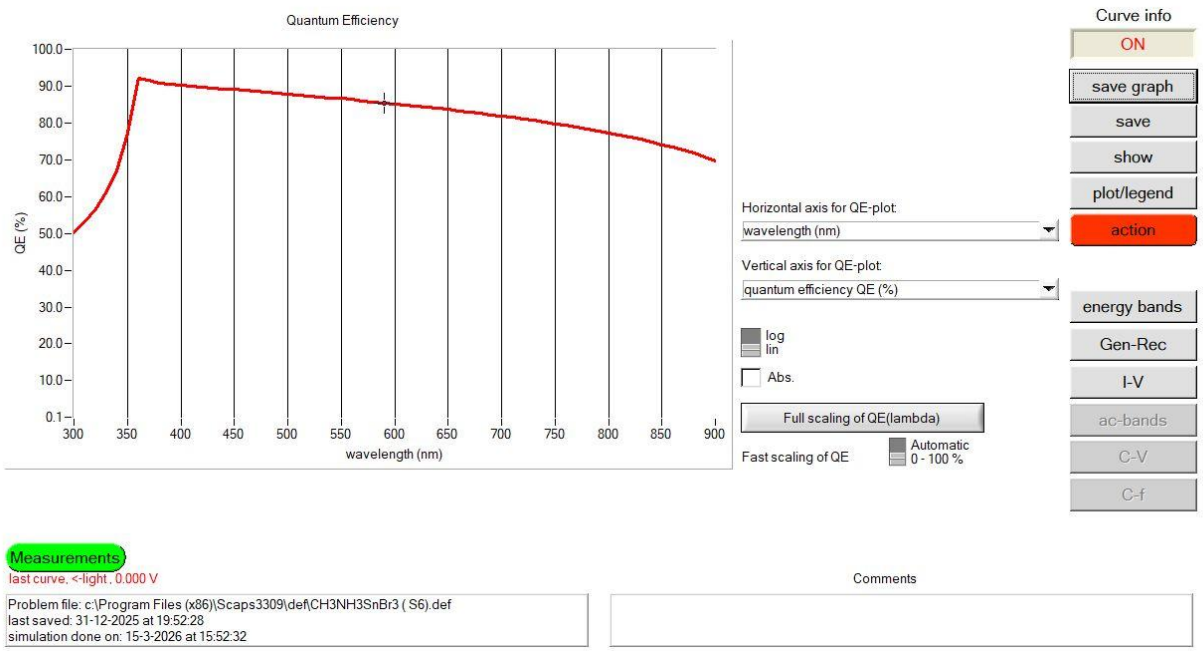

7um Qe

Figure 10: QE spectra for absorber thickness variation

In Figure 11 the recombination behavior is further examined and it is found that recombination current is higher in the case of a greater absorber layer. This proves that a thick sample will result in higher bulk recombination, which will limit the performance of the device.

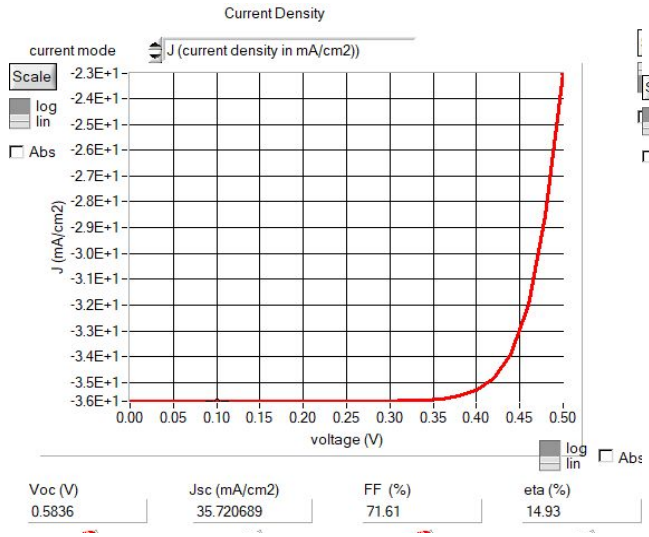

0.3um

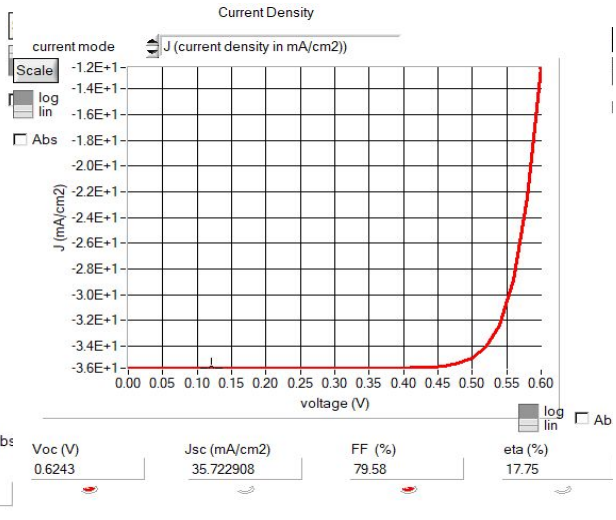

0.7um

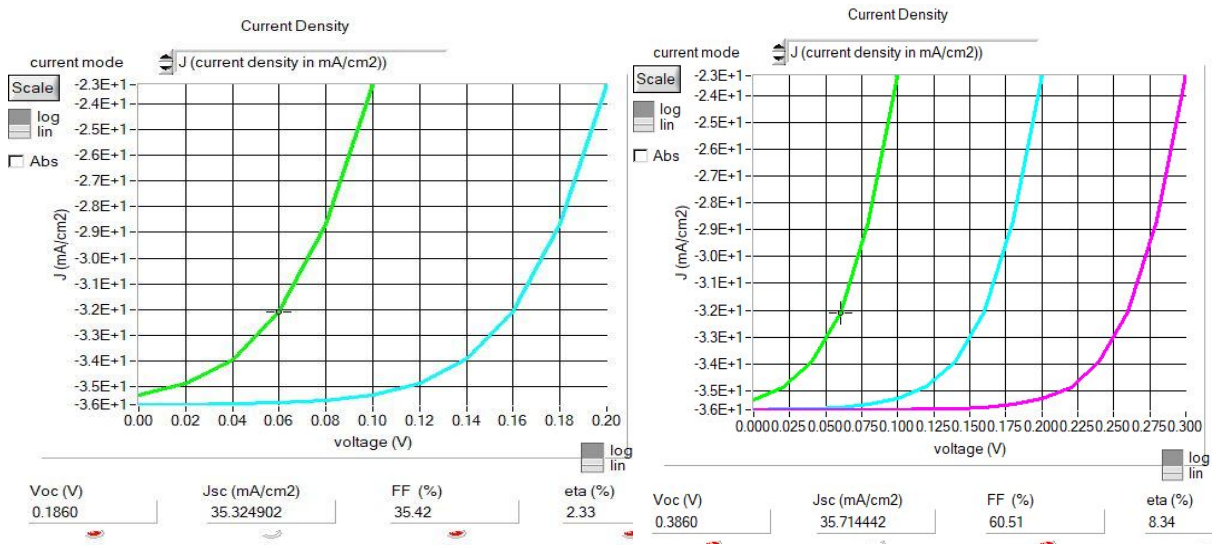

1um **3um**

Figure 11: Recombination current versus absorber thickness

3.3.2 Back Contact Metal Analysis

Figure 12 compares J V characteristics of Au, Cu, Ag, and Fe demonstrating how different back contact metals on the performance of the device. Among them, gold (Au) has the best performance because it has the best work function alignment that allows the extraction of holes to be made easier. On the other hand, Fe is the least efficient with low band alignment and recombination.

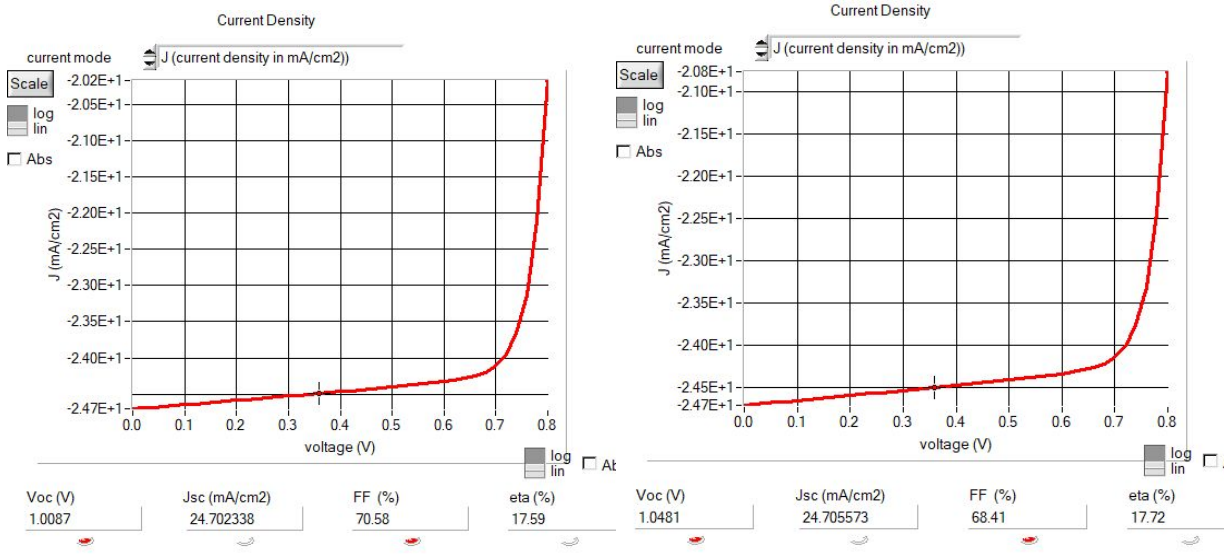

Cu **Au**

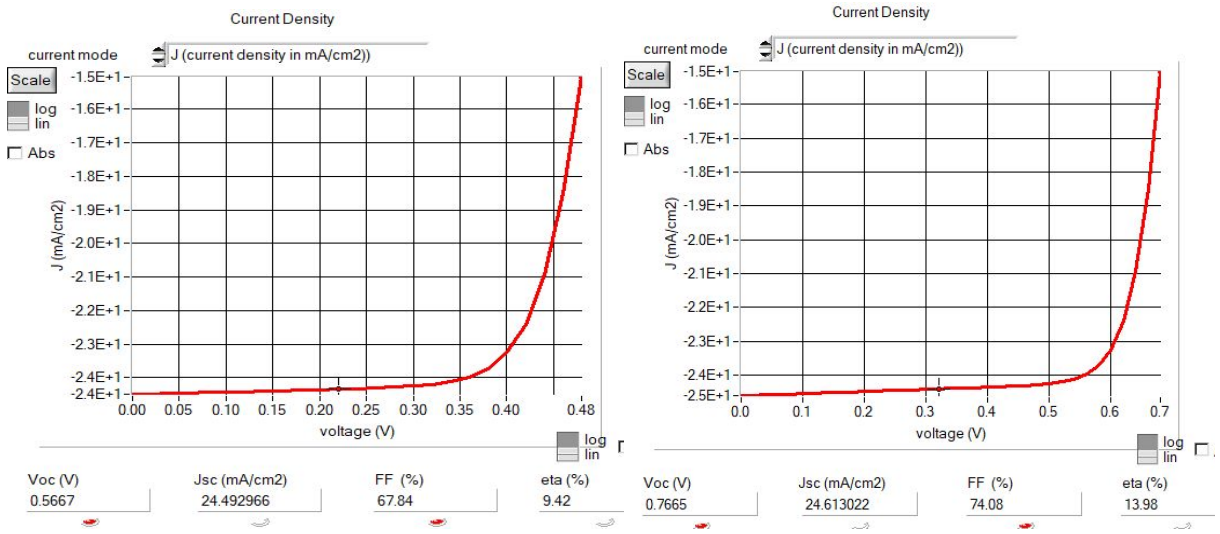

Graphene **Fe**

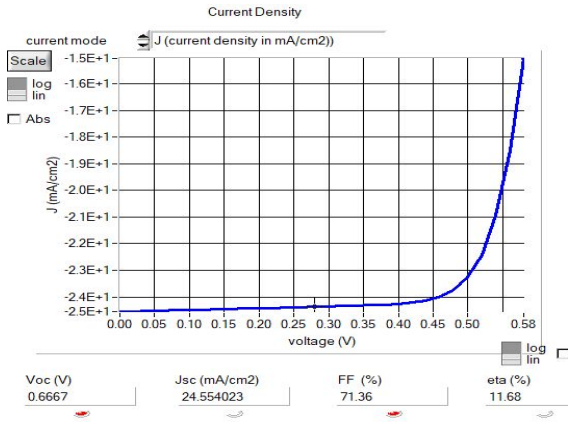

Ag

Figure 12: J–V characteristics for different back contact metals (Au, Cu,Graphene, Ag, Fe)

Figure 13 demonstrates recombination property of various metals. It is noted that recombination is minimal in the case of Au and maximum in the case of Fe which proves that contact engineering is a pivotal element in reducing recombination losses.

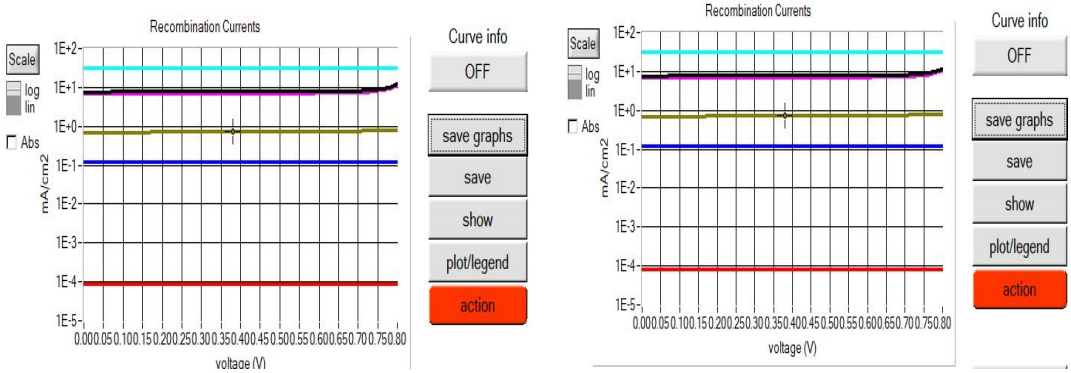

Cu **Au**

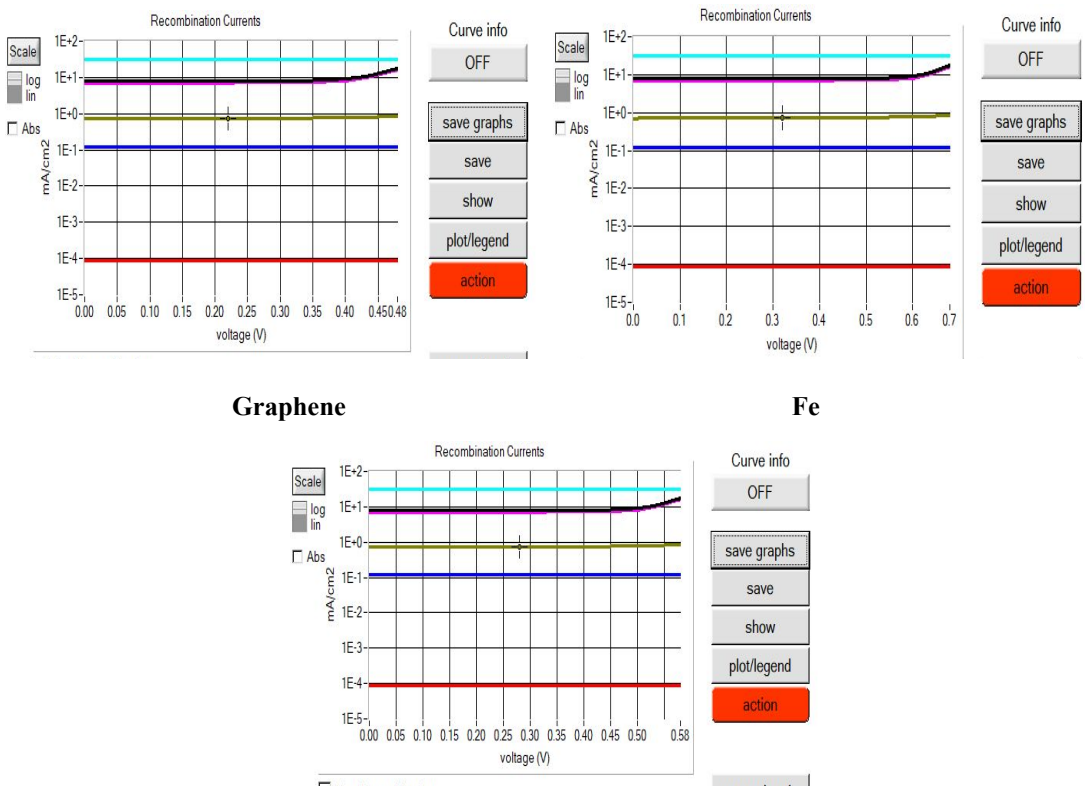

Graphene **Fe**

Ag

Figure 13: Recombination comparison for different back contact metals

3.3.3 Transport Layer Optimization (FTO, TiO_2, Spiro-OMeTAD)

Figure 14 demonstrates the influence of the thickness of the FTO variation on the performance of the device. Optimized FTO thickness is found to enhance series resistance and improve conductivity resulting in better Voc and and Jsc.

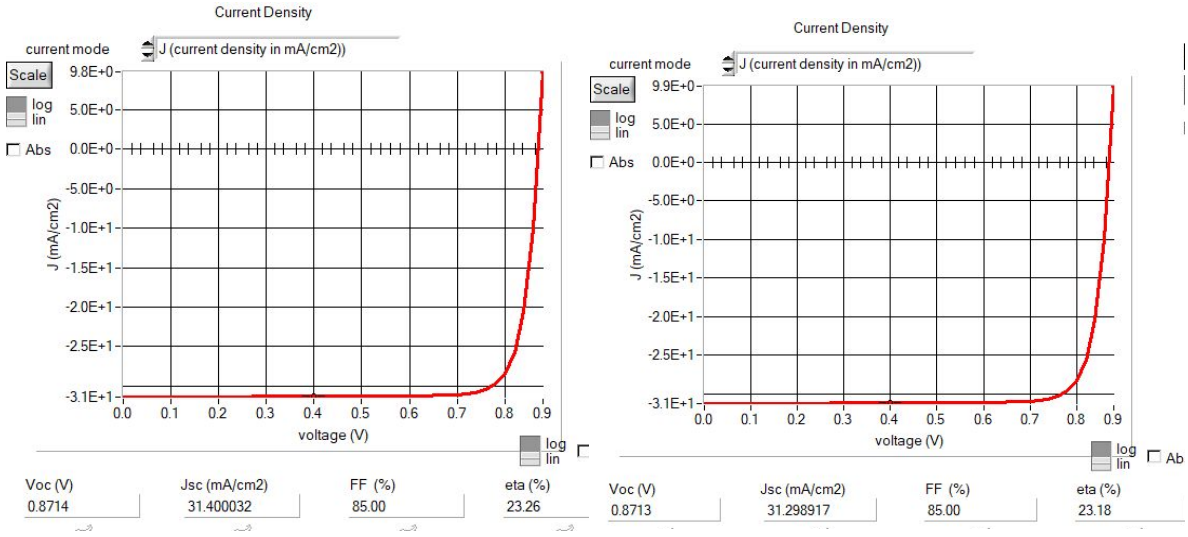

0.1 um **0.5 um**

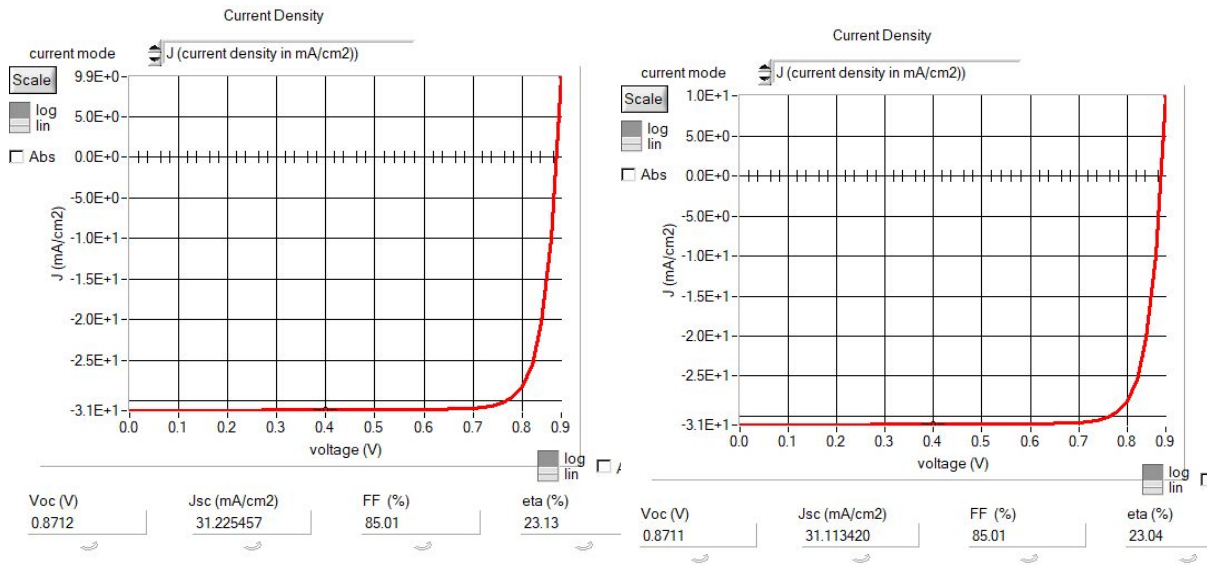

1um **3um**

Figure 14: J–V characteristics for FTO layer variation

Figure 15 shows the effect of TiO 2 thickness (ETL). A parasitic thickness optimum increases electron transport and minimizes recombination losses. In addition to the optimum value, there is a performance loss with high resistance.

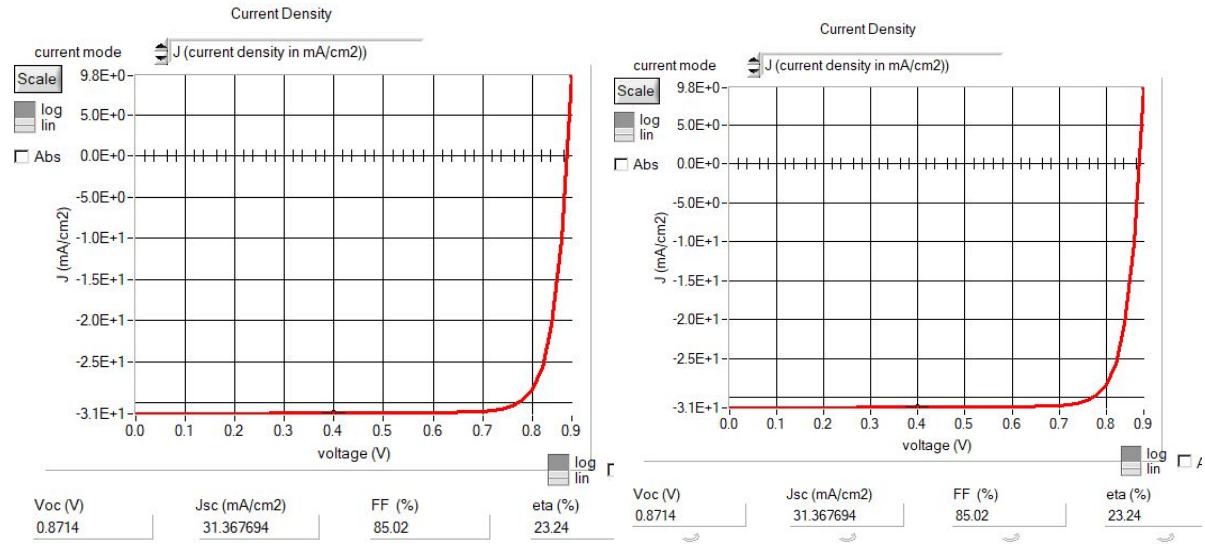

0.5um **1um**

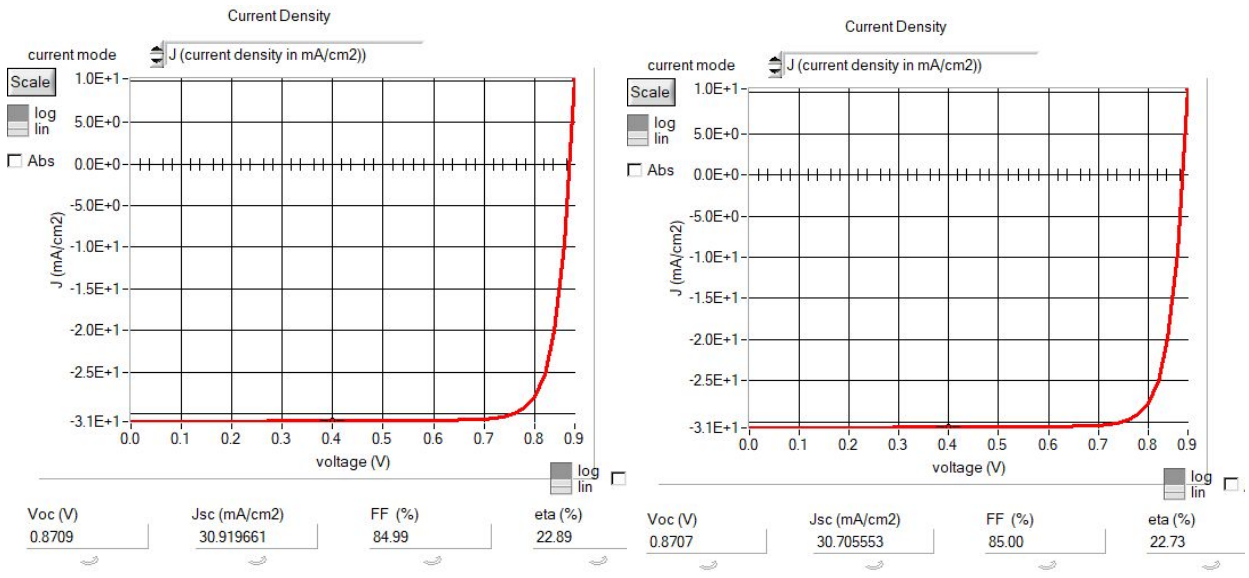

3um **5um**

Figure 15: J–V characteristics for TiO_2 thickness variation

The same applies to the impact of the thickness of Spiro-OMeTAD (HTL), which is shown in Figure 16. This efficiency rises with thickness to an optimum (c. 10 µm) and then reduces as the resistive losses increase.

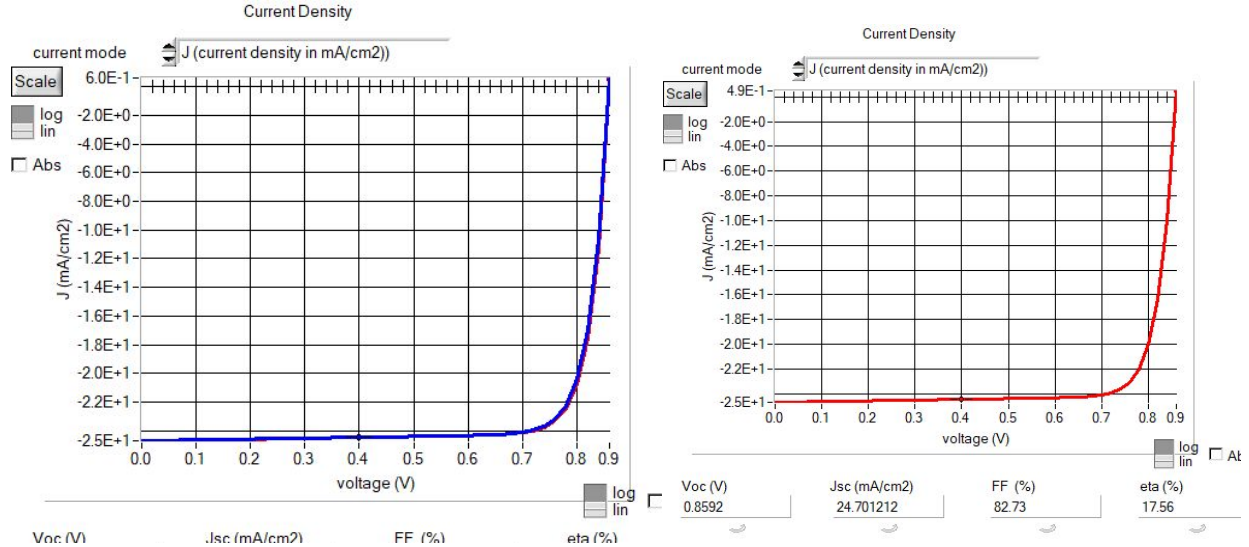

5um **10um**

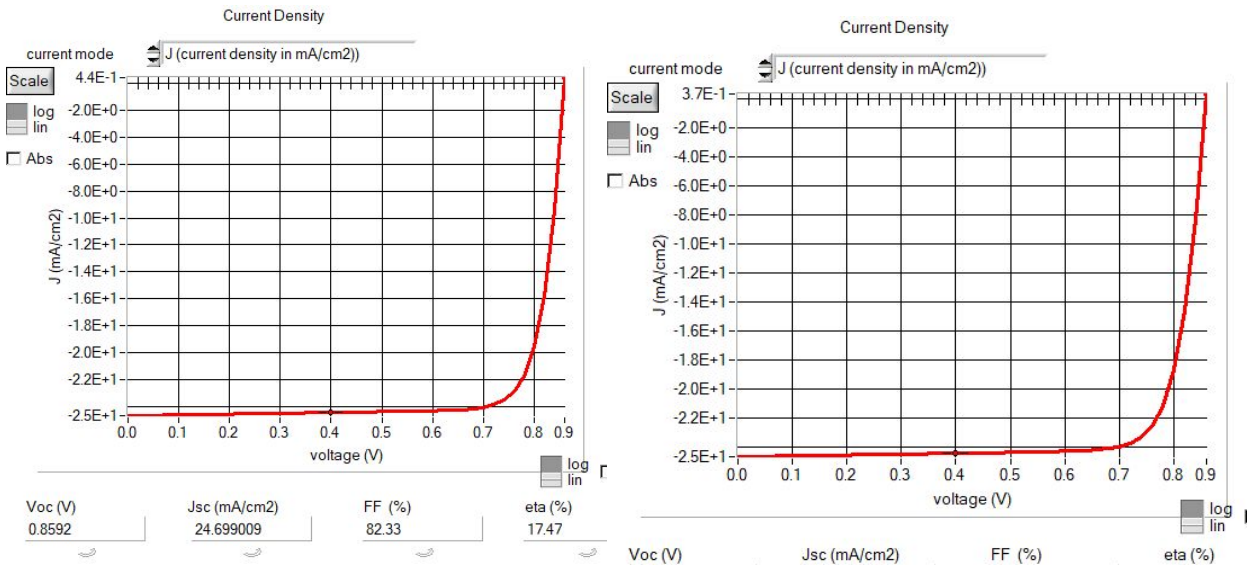

15um **25um**

Figure 16: J–V characteristics for Spiro-OMeTAD thickness variation

3.3.4 Temperature Analysis

Figure 17 shows the JV characteristics of the temperature-dependent device. It is noted that the performance of devices reduces with rise in temperature, mainly because of augmentation of recombination and carrier scattering.

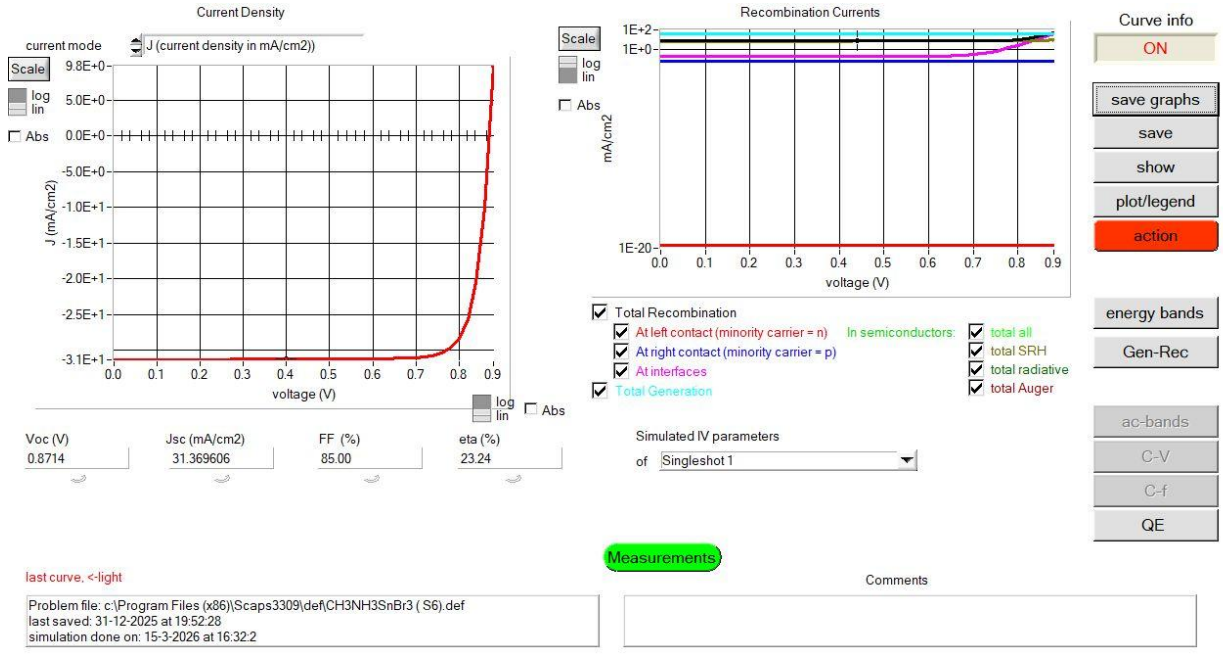

300

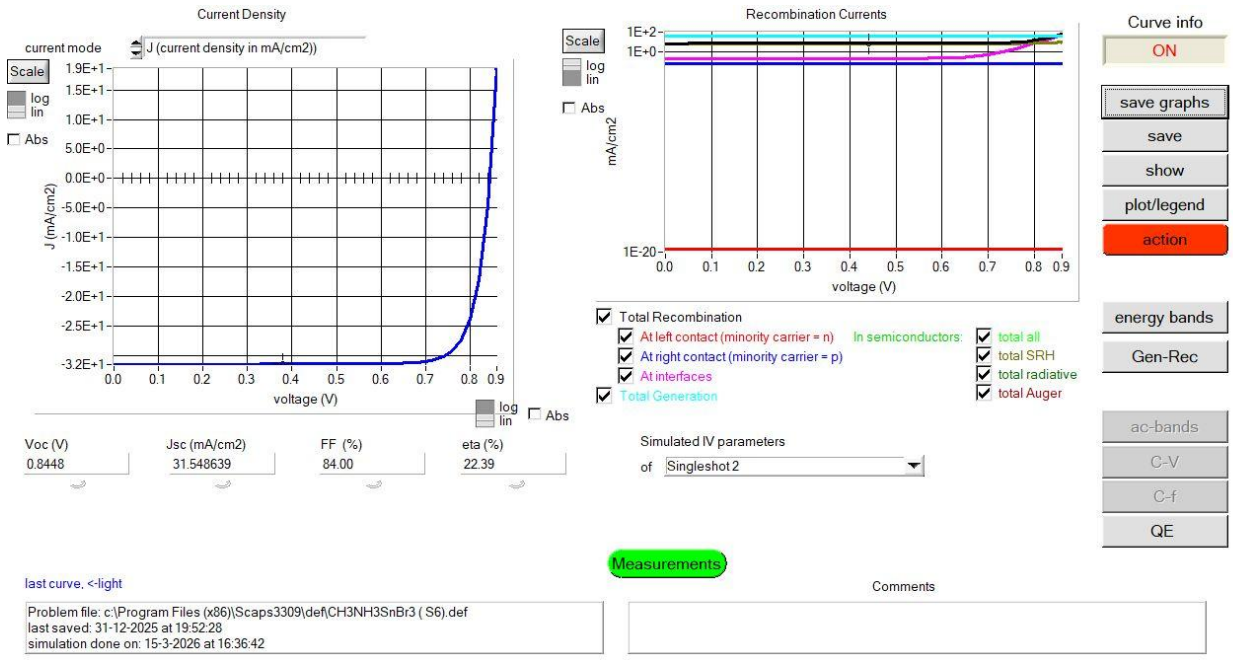

320

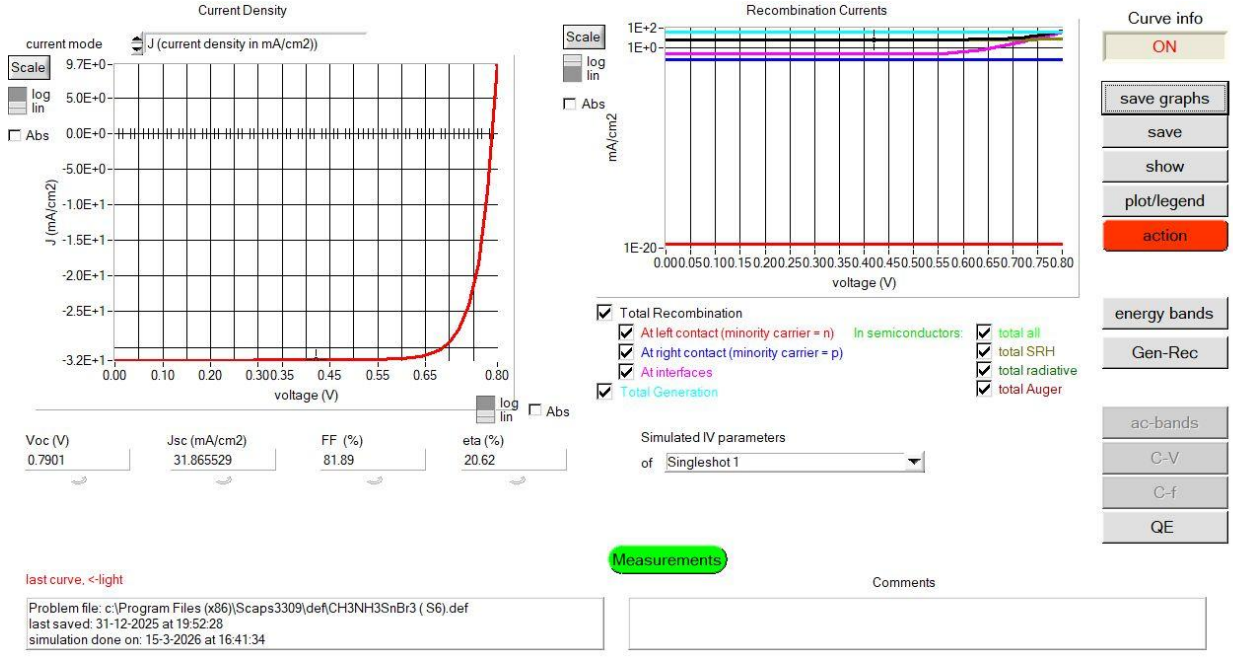

Graphen 360

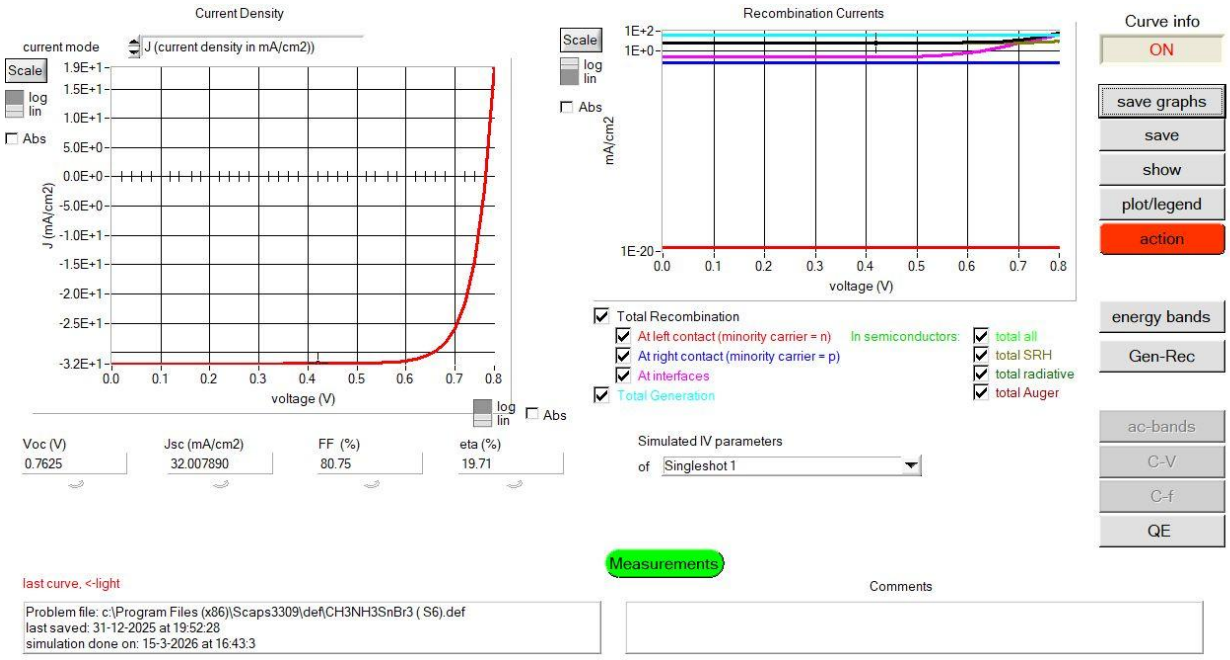

380 Fe

Figure 17: Temperature dependent J–V characteristics

Table 5: Summary of Model 3 Performance

Parameter	Value
Voc (V)	0.86 – 0.87
Jsc (mA/cm²)	31 – 32
FF (%)	84 – 85
Efficiency (%)	~23.2

The general outcomes found in Table 3.3 show that Model 3 is the most efficient of all the models because of the effective multi-parameter optimization, better carrier transport, and less recombination losses.

Table 6: Comparison of All Models

Model	Voc (V)	Jsc (mA/cm²)	FF (%)	Efficiency (%)	Key Limitation
Model 1	0.62–0.66	~37	~83	~19.33	Temperature sensitivity
Model 2	0.31–0.89	20–32	Low	~18.63	Recombination + low FF
Model 3	0.86–0.87	31–32	84–85	~23.2	Temperature stability

An overall optimization of the absorber thickness, transport layers, and back contact materials have a significant positive effect on the performance of the devices. “The optimal design reaches the highest efficiency of about 23.2 percent, which indicates the usefulness of multi-parameter optimization of the lead-free perovskite solar cell”.

Solar cell design needs to be efficient and this necessitates the contact materials, the thickness of the layers, charge transport, and thermal stability to be optimized at the same time, in order to ensure that recombination is minimized and the conversion efficiency is maximized.

4. CONCLUSION

This paper is a numerical research report examining three models of solar cell concentrated on the relationship between photovoltaic performance and material choice, device design, and operating environment. “The findings clearly show that charge transport mechanisms, recombination behaviour, and energy band alignment have a strong influence on the solar cell efficiency. The silicon-based device in Model 1 has stable and reliable performance and efficiency is largely determined by the back-contact materials. Carrier extraction and losses due to recombination are reduced by high work function metals like gold and copper and result in high open-circuit voltage and fill factor. Model 2 demonstrates the difficulties which are attributed to the lead-free perovskite solar cells”. Although the device has reached high optical absorption and high quantum effectiveness, it still has low recombination rate and low charge transport, which limits the performance of the devices with low fill factor and efficiency. This implies that quality and control of defects of materials is a key aspect in enhancing lead-free devices.

The effectiveness of multi-parameter optimization is shown in model 3, which is able to achieve high efficiency. “The CH 3 NH 3 SnBr 3” device has the highest efficiency of all models (~23.2 percent) by optimizing absorber thickness, transport layers, and contact materials. Balanced carrier transport, minimized recombination losses, and optimized energy band alignment are credited to the improved performance. The temperature analysis of all models proves that the performance of the device reduces with the temperature because the recombination increases and the voltage output decreases. This highlights the significance of thermal stability in the design of solar cells.

All in all, the research indicates that high-efficiency solar cells do not rely on a single factor but a balanced methodology should be considered. The better choice of material, device design and thermal characteristics make their significance in performance improvement. Results can be useful in creating solar cells which are not only efficient but environmentally safe especially using lead free material.

5. Future Scope

Though the current work provides a good simulation-based insight into know how well a solar cell works, it has room to be improved and put into practical use. Further studies can be dedicated to the enhancement of the quality of lead-free perovskites materials by minimizing defects using more effective passivation methods or by compositional tuning. This would assist in reducing trap states and enhancing carrier lifetime. The other significant field is interface engineering. Further minimization of recombination losses and better charge extraction can be achieved by maximizing the amount of band alignment among the absorber plus transport layers. Besides this, the stability studies should be conducted over a long period and in real environmental conditions like different temperature, humidity, and constant light to determine the reliability of the devices.

The exploration of tandem or hybrid solar cell designs (particularly the combination of silicon with non-lead perovskites) to achieve even higher efficiencies than single-junction limits, is also a possibility. We will need to test the finding of the simulation experimentally to ensure practical feasibility. Lastly, parameter optimization by using machine learning and artificial intelligence can assist in making the design process more efficient and faster to find the most optimal parameters with a minimum of efforts.

Reference

1. Green, M. A., et al. Solar cell efficiency tables (version 51). Progress in Photovoltaics: Research and Applications, 26, 3–12 (2018).
2. Hosenuzzaman, M., et al. Global prospects, progress, policies, and environmental impact of solar photovoltaic power generation. Renewable and Sustainable Energy Reviews, 41, 284–297 (2015).
3. Kim, H., et al. Planar heterojunction organometal halide perovskite solar cells: Roles of interfacial layers. Energy & Environmental Science, 9, 12–30 (2016).
4. Fu, F., et al. High-efficiency inverted semi-transparent planar perovskite solar cells. Nature Energy, 2, 16190 (2016). Chen, R., et al. Efficient and stable inverted planar perovskite solar cells using HTM. ChemSusChem, 11, 1467–1473 (2018).
5. Heo, J. H., et al. Hysteresis-less $CH_3NH_3PbI_3$ perovskite solar cells with 18.1% efficiency. Energy & Environmental Science, 8, 1602 (2015).
6. Ratcliff, E. L., et al. Energy level alignment in NiOx-based solar cells. Organic Electronics, 13, 744–749 (2012).
7. Baena, J. P. C., et al. Highly efficient planar perovskite solar cells through band alignment engineering. Energy & Environmental Science, 8, 2928–2934 (2015).
8. Noh, M. F. M., et al. Electron transport layer architecture in perovskite solar cells. Journal of Materials Chemistry C, 6 (2018).
9. Sharma, S., et al. ZnO thin films for optoelectronic applications. Superlattices and Microstructures, 75, 378–389 (2014).

10. Tang, H., et al. Electrical and optical properties of TiO_2 thin films. Journal of Applied Physics, 75, 2042 (1994).
11. Herz, L. M. Charge-carrier mobilities in metal halide perovskites. ACS Energy Letters, 2, 1539–1548 (2017).
12. Dong, Q., et al. Electron–hole diffusion lengths >175 μm in perovskites. Science, 347, 967–970 (2015).
13. Hutter, E. M., et al. Carrier dynamics in perovskite solar cells. Journal of Physical Chemistry Letters, 6, 3082–3090 (2015).
14. Burgelman, M., Nollet, P., & Degrave, S. Modelling polycrystalline solar cells. Thin Solid Films, 361–362, 527–532 (2000).
15. Verschraegen, J., & Burgelman, M. Numerical modeling using SCAPS. Thin Solid Films, 515, 6276–6279 (2007).
16. Burgelman, M., et al. SCAPS Manual. University of Gent (2016).
17. Sawicka-Chudy, P., et al. SCAPS simulation of TiO_2/CuO solar cells. Materials Research Express, 6, 085918 (2019).
18. El-Naggar, A. A., et al. Performance enhancement of heterojunction solar cells via simulation. Scientific Reports, 14, 7614 (2024).
19. Pandey, R., et al. Non-toxic perovskite–silicon tandem solar cell (30.7% efficiency). ACS Applied Electronic Materials, 5, 5303–5315 (2023).
20. O'Regan, B., & Grätzel, M. Dye-sensitized solar cells. Nature, 353, 737–740 (1991).
21. Grätzel, M. Solar energy conversion by dye-sensitized cells. Inorganic Chemistry, 44, 6841–6851 (2005).
22. Fortunato, E., et al. Oxide semiconductor thin films. Advanced Materials, 24, 2945–2986 (2012).
23. Fortunato, E., et al. Transparent conducting oxides for photovoltaics. MRS Bulletin, 32, 242–247 (2007).
24. Rühle, S., et al. All-oxide photovoltaics. Journal of Physical Chemistry Letters, 3, 3755–3764 (2012).
25. Hussain, S., et al. Cu_2O/TiO_2 heterojunction solar cells. Thin Solid Films, 522, 430–434 (2012).
26. Pavan, M., et al. TiO_2/Cu_2O solar cells via spray pyrolysis. Solar Energy Materials and Solar Cells, 132, 549–556 (2015).
27. Morasch, J., et al. Bi_2O_3 thin films photovoltaic properties. Physica Status Solidi (a), 211, 93–100 (2014).
28. Nakamura, M., et al. Cd-free thin-film solar cells with 23.35% efficiency. IEEE Journal of Photovoltaics, 9, 1863–1867 (2019).
29. Dhakal, T. P., et al. CZTS thin film solar cell characterization. Solar Energy, 100, 23–30 (2014).